

BOTSWANA INTERNATIONAL UNIVERSITY
OF SCIENCE & TECHNOLOGY

A SYNTHESIS METHOD FOR QUALITY-FACTOR ENHANCED SUBSTRATE INTEGRATED INDUCTOR FOR L-S BAND

A THESIS SUBMITTED TO THE FACULTY OF ENGINEERING AND TECHNOLOGY IN FULFILMENT OF THE REQUIREMENTS FOR THE AWARD OF THE DEGREE OF MASTER OF SCIENCE IN TELECOMMMUNICATIONS ENGINEERING OF
BIUST

OLEBOGENG BONE KOBE

SEPTEMBER 2017

A SYNTHESIS METHOD FOR QUALITY-FACTOR ENHANCED SUBSTRATE INTEGRATED INDUCTOR FOR L-S BAND

OLEBOGENG BONE KOBE

Registration No: 14100212

BSc (Telecommunications) (Oxford Brookes University)

Electrical, Computer and Telecommunications (ECT),

Faculty of Engineering and Technology (CET),

Botswana International University of Science and Technology

olebogeng.kobe@studentmail.biust.ac.bw

A Thesis Submitted to the Faculty of Engineering and Technology (CET)
in Fulfilment of the Requirements for the Award of the Degree of Master of Science in
Telecommunications Engineering of BIUST

Supervisor(s): Prof. Joseph Chuma

Electrical, Computer and Telecommunications

College of Engineering & Technology, BIUST

chumaj@biust.ac.bw, +2674900117

Signature: _____ Date: 22/11/2017

September, 2017

Copyright © Olebogeng Kobe, 2017

DECLARATION AND COPYRIGHT

I, Olebogeng Bone Kobe, declare that this dissertation/thesis is my own original work and that it has not been presented and will not be presented to any other university for a similar or any other degree award.

Signature .....

This dissertation/thesis is copyright material protected under the Berne Convention, the Copyright Act of 1999 and other international and national enactments, in that behalf, on intellectual property. It must not be produced by any means, in full or in part, except for short extracts in fair dealing; for researchers private study, critical scholarly review or discourse with an acknowledgement, without the written permission of the office of the Provost, on behalf of both the author and the BIUST.

CERTIFICATION

The undersigned certifies that he/she has read and hereby recommends for acceptance by the College of Engineering and Technology a dissertation/thesis titled: A SYNTHESIS METHOD FOR QUALITY-FACTOR ENHANCED ON-CHIP MICROWAVE RESONATOR FOR L-S BAND, in fulfilment of the requirements for the degree of Master of Science in Telecommunications Engineering of the BIUST.

……..	.....
Dr.	Dr.
(Supervisor)	(Co-Supervisor)
Date: ……..	Date: ……..

ABSTRACT

The thesis presents a flawless synthesis method for designing high quality factor (Q) on-chip microstrip resonator in the form of an inductor based on layout optimisation technique. While the layout optimisation method is already reported in the literature, it was only based on the turns of the spiral inductors with the width of the inner turn narrower than the width of the outer turn. Therefore, since resistivity is dependent of the conductor length and thickness, it is certain that the shorter and/or the thicker the conductor the lower the resistance. Consequently, the low resistance means reduced ohmic losses thus higher performance and higher-Q. Therefore, this optimisation method does not extensively consider ohmic losses relating to resistance of the conducting metal. Conversely, the proposed technique is an extended layout optimisation method developed to reduce ohmic losses of the conducting metal by varying the width of sequential segments, with the inner most segments narrower than the outer most segments of each turn of the spiral inductor. The application of this technique means that the width of each segment is different from that of the succeeding segment, thus making the width of a single spiral turn variable. The technique reduces ohmic losses caused by resistance of segments. It is substantiated that the resistance of a narrow conductor can be reduced by making the conductor short. Likewise, the resistance of a longer conductor can be reduced by making the conductor wider. Two structures, one possessing the traditional characteristics of former technique, and the other possessing the characteristics of the new proposal were built and simulated. The simulation results present higher current distribution in a variable segment width as compared to lower current distribution in a variable turn spiral. The higher the current flow the high the energy stored in the structure hence high Q-factor. The resultant Q-factor improvement observed was over 35% in comparison to the conventional fixed width model. Also a 11.57% improvement was observed compared to the original layout optimisation technique i.e. the variable turn width and spacing.

ACKNOWLEDMENT

I thank Almighty God for giving me good health and strength to finish this research project and accomplish the work and assignment that were expected of me by my supervisor and the Botswana International University of Science and Technology (BIUST) as a whole. I would also like to acknowledge my supervisor Prof. Joseph Chuma for his enduring support throughout this research project. Despite my struggles at the beginning, Prof Chuma's enduring support was my strength as he made sure he avail himself whenever I need his assistance. I appreciate his endless effort in making sure I achieve what I was looking for, which is to get my Masters of engineering degree. Special thanks goes to colleagues in the department of electrical, computer and telecommunications engineering (ECT) for their support and encouragement. I appreciate the help they offered me, big or small their input was useful and very significant. I would like to acknowledge BIUST University as a whole for provision of shelter for studies. Despite it being a newly established institution with limited resources, BIUST has been a home away from home. I thank BIUST staff, student and everyone else who made this happen. My last gratitude and appreciation is to my friends and family for their never-ending love and support, and most importantly for believing in me. Without everyone's input, directly or indirectly, this could have been a never-ending task.

LIST OF TABLES

Table 2.1 – Summary of latest developments in conductor layout optimise inductors 174
Table 2.2 – Summary of latest developments in PGS inductors..... 476
Table 2.3 – Summary of latest developments on differentially inductors..... 187
Table 2.4 – Summary of latest developments in spiral inductors with negative feedback 19
Table 3.1 – Q-value comparison at selected frequencies within the L-S Band 473
Table 3.2 – Dimensions of the two models (VTW vs. VSW model)..... 476
Table 3.3 – Dimensions of the two models (VTW vs. VSW model)..... 476
Table 3.4 – comparison of current results with existing similar work..... 477

LIST OF FIGURES

Figure 1.1 – Microstrip geometry (a) cross-sectional view (b) top view and (c) equivalent lumped-element model 2
Figure 1.2 – Forms of spiral inductors 2
Figure 1.3 – An equivalent model for terminal grounded inductor for Q-modelling 3
Figure 1.4 – Lumped-element model of a resonator a) series and b) parallel configuration 5
Figure 1.5 – Q response of a resonating circuit 8
Figure 2.1 – Typical negative resistance/conductance generators 195
Figure 2.2 – Typical negative resistance/conductance generators 198
Figure 2.3– Temporary bonded carrier for silicon substrate thinning process 210
Figure 3.1 – Square spiral geometry 384
Figure 3.2 – Square spiral with variable segment W&S 386
Figure 3.3 – (a) Parallel current carrying spiral segments modelling proximity effect (b) segment cross-sectional view 29
Figure 3.4 – Schematic representation of electrically and magnetically induced currents 29
Figure 3.5 – Equivalent circuit model of spiral segments 380
Figure 3.6 – Graph of Q versus frequency of VTW and VSW spirals 382
Figure 3.7 – Self-resonance factor of a VTW and VSW structure 384
Figure 3.8 – Substrate loss factor of a VTW and VSW structure 384
Figure 3.9 – CST model of a VTW Spiral Inductor 38
Figure 3.10 – Surface Current Distribution in a VTW model 387
Figure 3.11 – Electric Field Distribution in a VTW model 387
Figure 3.12 – Magnetic Field Distribution in a VTW model 398
Figure 3.13 – Power simulated vs. power lost on a VTW model 39
Figure 3.14 – S-parameters of a VTW model 410
Figure 3.15 – Quality-factor ASCII Export file from CST MWS (VTW model) 380
Figure 3.16 – CST models of a VSW Spiral Inductor 421
Figure 3.17 – Surface current distribution in a VSW model 382
Figure 3.18 – Electric Field Distribution on a VSW model 382
Figure 3.19 – Magnetic Field Distribution on a VSW model 383

Figure 3.20 – Power simulated vs. power lost on a VSW model 384
Figure 3.21 – Scattering Parameters of a VSW model..... 385
Figure 3.22 – Quality-factor ASCII Export file from CST MWS(VSW model)..... 385

LIST OF ABREVIATIONS

$+R_s$ – Positive Resistance

3D – 3 Dimensional

ASCII – American Standard Code for Information Interchange

BiCMOS – Bipolar CMOS

BW – Bandwidth

CMOS – Complementary Metal Oxide Semiconductor

C_p – Coupling Capacitance

C_s – Series Capacitance

CST – Computer Simulation Technology

E_e – Electric Energy

EM – Electromagnetic

E_m – Magnetic Energy

EMC – Electromagnetic Compatibility

FEM – Finite Element Method

FIT – Finite Integration Technique

F_R – Self Resonance Factor

FR-4 – Flame Retardant 4

F_S – Substrate Loss Factor

f_{SRF} – Self Resonance Frequency

GA – Genetic Algorithm

GaAs – Gallium Arsenide

HFSS – High Frequency Structure Simulator

HR-Si – High Resistive Silicon

IC – Integrated Circuit

IEEE – Institute of Electrical and Electronics Engineers

L_s – Series Inductance

LTCC – Low Temperature Co-fired Ceramic

MIC – Microwave Integrated Circuit

MW – Microwave

P – Power

PCB – Printed Circuit Board

Q – Quality Factor

Q_e – External Quality Factor

Q_L – Loaded Quality Factor

Q_u – Unloaded Quality Factor

RF – Radio frequency

RFIC – Radio Frequency Integrated Circuit

R_p – Coupling Resistance

$-R_s$ – Negative Resistance

R_s – Series Resistance

SiO_2 – Silicon Dioxide

VCO – Voltage Controlled Oscillator

VSW – Variable Segment Width

VSWR – Voltage Standing Wave Ratio

VTW – Variable Turn Width

TABLE OF CONTENTS

CHAPTER ONE **1**

BACKGROUND 1

OVERVIEW 4

Lumped element 5

Quality factor 6

MOTIVATION 9

PROBLEM STATEMENT 10

OBJECTIVES 10

Q-factor enhancement 10

Conductor loss reduction 11

HYPOTHESIS/RESEARCH QUESTION 11

SIGNIFICANCE OF RESEARCH/CONTRIBUTION 12

OUTLINE 12

CHAPTER TWO **13**

TRENDS IN SPIRAL MODELING 13

DESIGN MODEL ANALYSIS FOR LOSS COMPENSATION 13

Conductor layout optimization 13

Pattern Ground Shield 14

Differential Excitation 16

Negative Resistance 17

SUBSTRATE MATERIALS 20

ELECTROMAGNETIC DESIGN AND SIMULATION TOOLS 21

High frequency structure simulation (HFSS) 21

Sonnet Suite 21

CST Microwave Studio 22

Optimizers for EM structures 22

CHAPTER THREE **24**

ELECTROMAGNETIC DESIGN AND ANALYSIS 24

CIRCUIT MODELLING AND OPTIMISATION 25
ANALYTIC MODELLING AND PROXIMITY EFFECT 28
NUMERICAL ANALYSIS AND RESULTS 32
ANALYTIC MODELLING AND PARAMETER EXTRACTION 35
ELECTROMAGNETIC SIMULATION 35
Variable Turn Width Spiral (VTW) 35
Variable Segment Width Spiral (VSW) 41
ANALYTIC CONCLUSION AND DISCUSSION (VTW VS. VSW MODEL) 46
Comparison to existing work 47
PUBLICATIONS 47
CHAPTER FOUR **49**
CONCLUSION 49
FUTURE RECOMMENDATION 50
REFERENCES ..... **i**
APPENDIX ..... **viii**
PUBLICATIONS viii
OPTIMISATION RUN viiii

1) CHAPTER ONE

1.1 BACKGROUND

In the early years of radio communications, rectangular waveguides were the most popular resonant structures due to their high-Q value. Despite bandwidth (BW) limitations, they were used to design high-Q devices with minimal power dissipation. The popularity of these resonant structures diminished as the demand for more miniaturised components continued to grow. Several other waveguide structures that exhibit greater BW and miniaturisation were developed. Among these were ridge waveguides which offered both great BW and smaller structure size. The ridge waveguide consist of at least one longitudinal internal ridges that serve primarily to increase transmission BW [1]. Following the ridge waveguide development, a new structure in coaxial line was used, providing the much needed miniaturisation capability and wide BW. However, this structure was limited by the lack of longitudinal component of field which made it difficult to create components using it. In an attempt to reduce the limitation of a coaxial line, Robert M. Barrett [2] modified it to design what was known as a stripline. Similar to a coaxial line, the stripline had zero cut-off frequencies. However, the popularity of the stripline was cut short by further modifications that lead to the current microstrip. The first microstrip developments were done shortly after the appearance of Barrett's article in the early 1950s, and it was presented as a competing printed circuit line [1]. In its simplest form, a microstrip resonator consists of two metal conductors separated by a dielectric substrate as illustrated in Figure 1.1. The suspended metal conductor on top of the substrate is a strip-line whereas the bottom conductor plate is a ground plane. The material separating the two conductors is a dielectric substrate of a dielectric constant (ε_r).

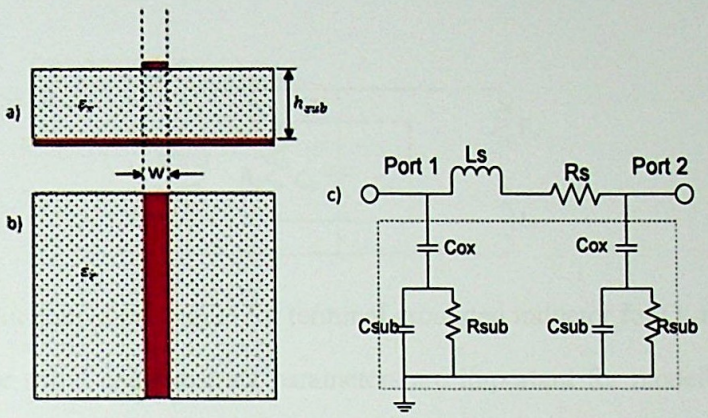


Figure 1.1 – Microstrip geometry (a) cross-sectional view (b) top view and (c) equivalent lumped-element model

The microstrip line is a basic component used to develop microstrip inductors which exist in various forms as illustrated in Figure 1.2. The inductor with least number of sides is a square spiral, whereas the inductor with infinite number of sides is a circular spiral, and between the two lies a variety of shapes such as hexagonal, octagonal etc. The square spiral is known to have a high inductance value but a low-Q value due to current crowding effect on the corners, and the circular spiral is known to have a lower inductance value but a higher-Q value. A circular spiral uses less chip area while making use of large chunks of metal conductors which reduces the R_s [3]. Despite its better-Q due as a result of lower R_s, the circular spiral is less popular since it is difficult to layout compared to other shapes. This limitation makes the square spiral more popular since it is easy to layout.

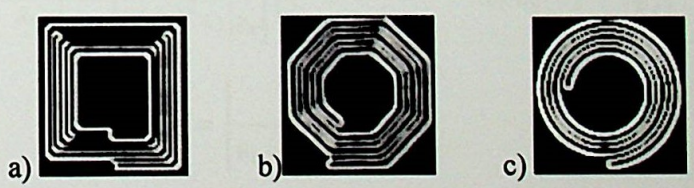


Figure 1.2 – Forms of spiral inductors

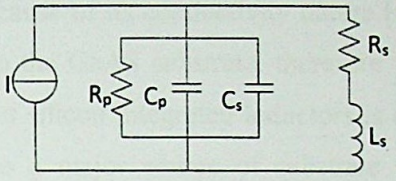


Figure 1.3 – An equivalent model for terminal grounded inductor for Q-modelling [4]

While both the spiral and substrate parameters are important for modelling-Q of the structure, at low frequencies the substrate-loss factor (F_S) and the self-resonance factor (F_R) are almost equal to unity, therefore only the magnetic energy stored by the inductor is important for Q-evaluation. This implies that the shunt branch in the circuit of Figure 1.3 is eliminated for Q-formulation thus leading to the intrinsic Q given by equation (1).

$$Q = \frac{\omega_o L_s}{R_s} \tag{1}$$

where ω_o, L_s, R_s are the resonance frequency in radians, series inductance and series resistance respectively. The ultimate-Q is then given by equation (2) as in [5], where an increase in frequency will result in significant reduction in Q value. This is due to the effect of the F_S and F_R in equations (3) and (4) respectively.

$$Q = \frac{\omega_o L_s}{R_s}\left[\frac{R_p}{R_p+\left[\left(\frac{\omega_o L_s}{R_s}\right)^2+1\right]R_s}\right]\left[1-\frac{R_s^2(C_s+C_p)}{L_s}-\omega_o^2 L_s(C_s+C_p)\right] \tag{2}$$

$$F_S = \left[\frac{R_p}{R_p+\left[\left(\frac{\omega_o L_s}{R_s}\right)^2+1\right]R_s}\right] \tag{3}$$

$$F_R = \left[1-\frac{R_s^2(C_s+C_p)}{L_s}-\omega_o^2 L_s(C_s+C_p)\right] \tag{4}$$

where C_p, R_p and C_s are the coupling capacitance, coupling resistance and series capacitance between the metal lines respectively [4]. The limiting factor in microstrip-Q is the R_s of metallisation. Other factors contributing to these limitations are conductive substrate losses normally from 1 to 10 Ω-cm. This is more common in the

silicon based substrates because of its conductivity nature [6]. Silicon substrates have low resistivity compared to the GaAS substrate, therefore the most vital degradation factor in the performance of silicon integrated inductors is the substrate losses. While capacitive coupling is also a major source of substrate losses the main cause of substrate loss is the inductive coupling normally caused by the magnetic fields entering the substrate, inducing eddy currents [7], [8] on the substrate material. Eddy currents increase the substrate losses and this reduces the performance and Q of the spiral. Due to the planar geometry of the inductor, these magnetically induced currents penetrate the silicon substrate inducing some currents loops within the substrate. However, the effects are predominant in the large area inductors, therefore they are suppressed by the development of silicon micromachining technique which is well-suited with ordinary silicon technologies [9].

1.2 OVERVIEW

Resonators, whether distributed or lumped-elements [10] allow for the exchange of electric and magnetic energies with low loss. While lumped element resonators are employed at radio frequencies (RF) ranging up to 300 MHz [11], their dimensions are comparable to the size of a wavelength at higher frequencies. For these reasons, it is almost impossible to design RF circuits using lumped elements at high frequencies. However, the difficulty leads to the use of integrated circuits (ICs) which offer capability to fabricate small devices. Despite positive outcomes from the IC technology, miniaturised circuits exhibit poor power handling capacity and a very low-Q. This is a common limitation for miniaturised distributed circuits, including on-chip resonators such as microstrip patch antennas and spiral inductors. Generally, on-chip resonators are distributed elements that can be represented in a lumped element model for analytic purposes. These are circuits composing of resistive, inductive and capacitive (RLC) components which can either be analysed in series or parallel configurations as illustrated in Figure 1.4. The interconnection of the lumped-elements results in energy storage and oscillation at ω_o. At this frequency, the capacitor and inductor store the electric and magnetic energy respectively. For a microstrip resonator, the magnetic energy is of utmost importance as it defines the resonator's Q.

The Q itself determines the performance of the resonator, and it is defined as the ratio of the energy stored to the total energy dissipated per unit cycle for a sinusoidal excitation [12]. This is represented by equations (5)–(7) as in [12]–[16], where E_m is the maximum magnetic energy stored, E_e is the maximum electric energy stored and P_{diss} is the average power dissipated. The symbol Q_u represents the unloaded-Q while ω is frequency in radians. Q_u is an important parameter of a resonant circuit and it is systematically discussed in subsequent sections.

$$Q_u = \omega \frac{Average\ Energy\ stored}{Average\ Energy\ lost\ per\ cycle} \tag{5}$$

$$Q_u = 2\pi \frac{E_m - E_e}{P_{diss}} \tag{6}$$

$$Q_u = -\frac{Im(y_{11})}{Re(y_{11})} \tag{7}$$

1.2.1 Lumped-Element Model

The RLC circuits are fundamental components in many RF applications such as filters and voltage controlled oscillators (VCO). While C and L store electric and magnetic energy respectively, R is an energy dissipating component. It provides stability with minimal damping during oscillation.

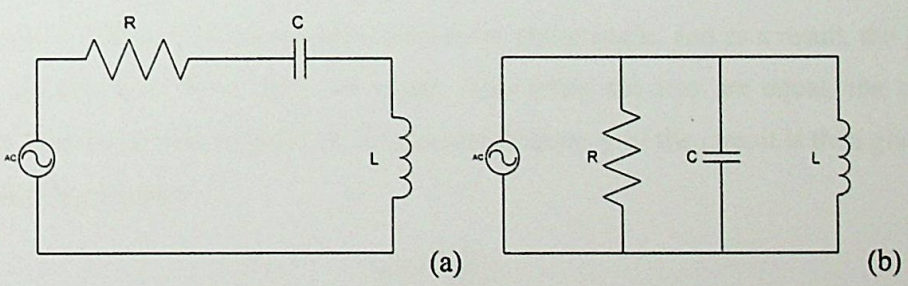


Figure 1.4 – Lumped-element model of a resonator a) series and b) parallel configuration

Considering a series resonant circuit in Figure 1.4 (a), at zero frequency, the impedance of the capacitor is infinite leading to an open circuit whereas the impedance of the inductor is very low leading to a short circuit. An increase in frequency decreases and increases the impedance of inductor and capacitor respectively relative

to the impedance of the resistor, thus the source voltage divides between the resistive impedance and the capacitive and inductive impedance. This leads to a smaller voltage at the output compared to the source voltage. Then at infinitely high frequency, the capacitive impedance is zero, thus presenting short circuit behaviour to the capacitor. On the other hand, the inductive impedance is infinite resulting in an open circuit, thus leading to significant voltage at the output [17]. The total impedance of the circuits in Figure 1.4 (a) is therefore given by equation (8).

$$Z_{total} = R + j\omega L + \frac{1}{j\omega C} \tag{8}$$

As the frequency increases, the integrated inductor traces start to exhibit significant capacitive effects with adjacent traces and the substrate. These additional capacitive effects change the inductor's behaviour to that of a second-order system, thus exhibiting a frequency(ω_o) in equation (9), at which the inductive impedance and the capacitive impedance are equal. Various RF applications use on-chip inductors at resonance frequency and a precise and efficient metric of energy storage can be drawn from the BW [18] of the system. The impedance of the series circuit at resonance is very low, and the phase angle is equal to zero because of the equality in imaginary capacitive and inductive impedance which results in cancellation of the two components. These two components control the phase angle, and as a result, the phase angle remains zero when they are equal. Also when the two are equal, the circuit realises maximum current possible. The centre frequency of the circuit is then given by the following equation.

$$\omega_o = \frac{1}{\sqrt{LC}} \tag{9}$$

1.2.2 Quality Factor

A. Unloaded-Q

While Q has so many definitions, the most common definition is described by equations (5) and (6). Assuming a second-order RLC system, the poles are parameterized in terms of the damping ratio(ξ) and natural frequency (ω_n) where the

transfer function of the system is given by (10). The pole locations are divided into four damping classes, undamped, underdamped, overdamped and critically damped. For the undamped case $\xi = 0$, therefore the poles are given by $s = \pm j\omega_n$. For the underdamped case $0 < \xi < 1$, therefore the poles are given by $s = -\alpha \pm j\omega_d$ where ω_d is the damped natural frequency given by $\omega_d = \omega_n\sqrt{1-\xi^2}$ and α is a matching constant. For the critically damped case $\xi = 1$, therefore the poles are coincidence at $s = -\omega_n$. Lastly for the overdamped case, $\xi \geq 1$, therefore the poles are given by $s = -(\xi \pm \sqrt{\xi^2 - 1})\omega_n$. For these cases, the Q value of the system is redefined by equation (11) where $\Delta\omega = \omega_2 - \omega_1$, defining the -3dB BW illustrated in Figure 1.5. The relation between the resonance frequency (ω_o) and the poles is given by $\omega_d = \sqrt{\omega_o^2 - \alpha^2}$ [19].

$$T(s) = \frac{\omega_n^2}{s^2 + 2\xi\omega_n s + \omega_n^2} \tag{10}$$

$$Q = \frac{\omega_o}{\Delta\omega} \tag{11}$$

The Q definition in (11) relates ω_o to the BW of the system inconsiderate of the impedance or power ratio. Such a definition is applicable to the computation of Q of parallel and series RLC lumped-element configurations [20] as illustrated by equation (12).

$$Q_p = \omega_o CR = \frac{R}{\omega_o L} \tag{12}$$

$$Q_s = \frac{\omega_o L}{R} \tag{13}$$

For a parallel configuration in equation (12), the value of R has to be very high to force a current flow through the L and C elements, thus increasing the chance of energy storage. And for a series configuration in equation (13), R value has to be very small so that less energy is lost at the damping at resonance.

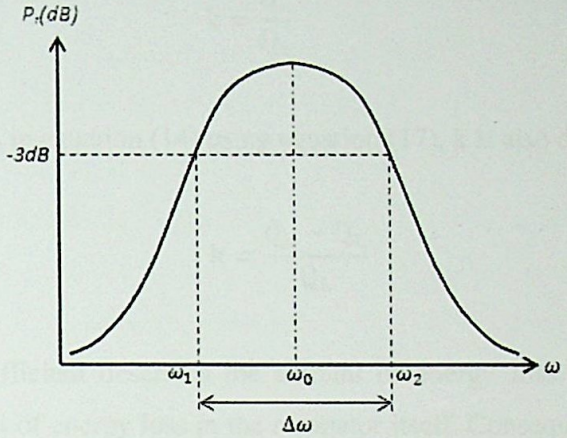


Figure 1.5 – Q response of a resonating circuit

B. Loaded-Q

Practically, resonators do not operate as independent circuits, but circuits coupled to other circuits in RF systems. The coupling of these resonant structures to external circuits introduces additional energy losses. This leads to reduced-Q commonly known as the loaded-Q (Q_L). The relationship between the Q_L and the Q_u is described by a common relation presented by equation (14), where Q_e represent the external-Q defined by equation (15) and P_e represents power dissipated by the external coupling and it is given by equation (16).

$$\frac{1}{Q_L} = \frac{1}{Q_u} + \frac{1}{Q_e} \tag{14}$$

$$Q_e = \omega \frac{E_m}{P_e} \tag{15}$$

$$P_e = \frac{1}{2} I_{max}^2 R \tag{16}$$

Commonly, a coupling coefficient denoted (k) is used to measure the degree of coupling between the resonator and the load circuitry connected to it [21]. The coefficient is defined by a Q relation described by equation (17).

$$k = \frac{Q_u}{Q_e} \tag{17}$$

Substituting for Q_e in equation (14) using equation (17), k is also defined as,

$$k = \frac{Q_u - Q_L}{Q_L} \tag{18}$$

The coupling coefficient describes the amount of energy loss in the external load against the amount of energy loss in the resonator itself. Consequently, there are three possible conditions associated to this power ratio, where power loss in the external circuitry is either large, less or equal to the power loss in the resonant circuit [22]. A condition where the Q_e is larger is referred to as under coupling, and in this case the coupling coefficient $k < 1$. For $k = 1$, then Q_e and Q_u are equal and the coupling is referred to as critical coupling. Lastly, if Q_e is smaller than Q_u of the resonator, the coupling is referred to as over coupling and $k > 1$.

1.3 MOTIVATION

High-Q on-chip inductors play a major role in the design of high performing RF integrated circuits (RFICs) and microwave integrated circuits (MICs). They have been extensively used in various applications at lower and intermediary frequencies, and these include sensors, oscillators, power converters and filters.

The performance of these RF and MW components tremendously ruined by conductor and substrate losses, with parasitics causing capacitive coupling which also has effect on the overall performance [9]. In addition, eddy currents from adjacent conductors causes high power dissipation at higher frequencies, thus leading to low-Q. Due to these effects, resistivity and dielectric loss has become more crucial substrate parameters that need to be taken into consideration when designing high-performing on-chip device.

With the increasing demand for designing low power and high frequency circuits, various applications such as impedance matching, tank circuits and bias chokes have

gained popularity and are widely used for low noise amplifiers, VCOs and power sources respectively [19]. It is quite common that this small RF devices are packaged with other circuits within metallization layers of an active die and board-level integration in what is commonly known as "on-chip" fabrication.

Various materials such as flame retardant 4 (FR-4) and silicon are widely used for the surface mount of these inductors. Owing to its high thermal conductivity, silicon has been the most commonly used material for fabrication of these on-chip devices [23]. Most commonly, silicon oxide (SiO_2) has been used for suspension of these devices on silicon substrate. With the SiO_2 layer present, the flexibility of using HR-Si exists hence significant reduction in substrate losses is achieved. The HR-Si is capable of presenting an effective resistivity of 3kΩ.cm for considerable low loss suitable for RF and microwave applications [24].

Regardless of their limitations, spiral inductors are extensively used in integrated circuits design as they provide miniaturisation for high level integration of components. As a result intense research is carried out to devise synthesis methods to alleviate these limitations, and in recent years, silicon micromachining techniques [25]–[27], have been applied in order to remove the integration substrate, and the technique proved to be vital in improving the Q and self-resonance frequency (f_{SRF}) of the inductor [9]. Another method with significant advantages is the "on-package" integration technique, in which the inductor and associated RF circuits are immersed within the metallization layers of the packaging chip such as in Low-Temperature Co-fired Ceramic (LTCC) [28]–[33].

1.4 PROBLEM STATEMENT

Despite tremendous research work carried out for several years, spiral inductors still suffer high losses and low-Q. However, the demand for these RF components continues to grow due to rapid growth in applications that utilise them. Reported for the first time in the past twenty years [9], the layout optimisation technique has been inadequately investigated particularly on the simplest form of spiral, the square spiral. This has only covered the multilayer spiral technique and the variable conductor width

and coil spacing technique which was only focused on optimising metal width by varying from turn to turn. While these two techniques have some positive results on the field distribution and power dissipation, there is still a room for improvement considering the fact that the spiral layout and conductor dimensions plays a major role in the ohmic losses associated to conductor and substrate losses.

1.5 OBJECTIVES

1.5.1 Q-factor enhancement

The main objective of this work is to devise a synthesis method to improve the quality factor of a microstrip inductor. In order to achieve this, there is a need to develop a design method which can preserve the energy generated in the resonator, to minimize the energy loss. This leads to the second objective in conductor loss reduction, to minimize ohmic losses and substrate related conduction losses.

1.5.2 Conductor loss reduction

Conductor layout plays a major role in energy storage and energy dissipation of a resonator. The induction of eddy currents at the centre and between the conductor traces is highly dependent on the design and layout of the conductor. Wider conductor traces increase the capacitive coupling between the conductor and the substrate, thus increasing the amount of displacement currents within the substrate. These also reduce the self-resonance frequency of the resonator. Therefore, narrower traces are necessary especially at the centre of the structure, leaving a wider inside diameter.

1.6 HYPOTHESIS/RESEARCH QUESTIONS

Conductivity of a material depends on its resistivity, where resistivity is an intrinsic property of a material and directly proportional to the total resistance (R), an extrinsic quantity that depends on the length and cross-sectional area of a resistor (resisting material). The resistance of an object depends on its shape and material of which it is composed. While highly conductive materials are used for fabrication of microstrip

inductors, their size and shape has a huge effect on their performance. Thin metal traces cause high resistive losses, whereas wide metal traces cause high electric field leading to high energy loss. All these lead to lower Q of the structure as a whole. An investigation into the layout of the structure may lead to a loss compensation solution, with reduced conductor losses and reduced capacitive losses. While the variable spiral-turn width and coil spacing technique yields some promising results, the technique could be extended to segmentation level, thus a variable spiral-segment width and coil spacing technique viable.

1.7 SIGNIFICANCE OF STUDY/CONTRIBUTION

The layout optimisation technique has been modified and extended to segmentation of the spiral model in order to reduce ohmic losses caused by the conducting metal, thus increasing the Q of the inductor. Formerly, the layout optimisation technique was investigated in [9], [12], but the investigation only considered the variation of spiral width from one turn to another. The extension of the technique considers variation of metal width from one segment to another which offers reduced resistance and higher Q. The outcome of the new investigation produces scattering parameters-S, Y and Z over a frequency band. While Q is directly calculated from the CST simulator, it can also be calculated from the Y and Z-matrices.

1.8 OUTLINE

This thesis is divided into four chapters. Chapter-1 introduces the background and principle of microstrip inductors as RF components.

Chapter-2 is a literature review, focusing more on the existing work as a way of data collection. This chapter discuss different techniques in spiral modelling and optimisation. It explains some loss mechanisms relating to spiral inductors and the influence of the layout parameters, including material type on spiral inductor performance and Q.

Chapter-3 introduces a proposed design technique for spiral inductors. A design method for square spiral inductor is presented. The spiral electromagnetic equations are expressed, and the layout technique is applied for optimisation to achieve high-Q within the L-S microwave band. The structural implementation of this proposed design is discussed, and numerical analysis is performed. This includes an electromagnetic simulation using CST MWS as well as results and discussion.

Lastly, Chapter-4 discusses conclusions drawn from the research and its findings from numerical and practical analysis undertaken. This also describes some of the lessons learned from this work and highlights future progress.

Chapter-3 introduces a proposed design technique for spiral inductors. A design method for square spiral inductor is presented. The spiral electromagnetic equations are expressed, and the layout technique is applied for optimisation to achieve high-Q within the L-S microwave band. The structural implementation of this proposed design is discussed, and numerical analysis is performed. This includes an electromagnetic simulation using CST MWS as well as results and discussion.

Lastly, Chapter-4 discusses conclusions drawn from the research and its findings from numerical and practical analysis undertaken. This also describes some of the lessons learned from this work and highlights future progress.

2) CHAPTER TWO

2.1 TRENDS IN SPIRAL INDUCTOR MODELLING

Spiral inductor fabrication came in the 1960s as a follow up of the microstrip concept first introduced by Robert M. Barrett in the early 1950s [2]. However, the components failed to gain popularity since they were not easy to integrate. These required a large chip area for practical inductance values considerable for microwave frequencies. Also, the components suffered low Q as a result of losses related to the heavily doped silicon substrates. Nonetheless, in the early 1990s, silicon on-chip inductors were designed, tested and reported by Nguyen and Meyer [34] in a 0.8μm silicon BiCMOS technology. They designed two square spirals of values 1.3 and 9.7nH with a peak Q-value of 8 and 3 at 4.1GHz and 0.9GHz respectively. The performance of the two spirals were tested and verified in LC-VCO and RF bandpass filter circuits, yielding promising results. Ever since, intense research on spiral inductors performance trends, design, optimisation, modelling and Q enhancement has been carried out and reported [12], [35]–[40] in literature. The application of these RF components continued to grow, and today their application is widely extended to higher frequencies including microwave and millimetre wave bands.

2.2 DESIGN MODEL ANALYSIS FOR LOSS COMPENSATION

2.2.1 Conductor Layout Optimisation

Layout optimisation method first appeared in the late 1990s when Craninckx and Steyaert discovered [41] that the largest contributor to high R_s at higher frequencies is at the innermost turns of the spiral. They discovered that the magnetic field induced by the current in the spiral conductor induces an electric field at the inner turns thus generating eddy currents. These currents affect the current distribution in the inner conductor making it inconsistently distributed thus increasing the series resistance. As a result, a new technique in layout optimisation was reported [9] in which the width of the metal trace for each turn is optimised by varying the width from turn-to-turn.

2) CHAPTER TWO

2.1 TRENDS IN SPIRAL INDUCTOR MODELLING

Spiral inductor fabrication came in the 1960s as a follow up of the microstrip concept first introduced by Robert M. Barrett in the early 1950s [2]. However, the components failed to gain popularity since they were not easy to integrate. These required a large chip area for practical inductance values considerable for microwave frequencies. Also, the components suffered low Q as a result of losses related to the heavily doped silicon substrates. Nonetheless, in the early 1990s, silicon on-chip inductors were designed, tested and reported by Nguyen and Meyer [34] in a 0.8μm silicon BiCMOS technology. They designed two square spirals of values 1.3 and 9.7nH with a peak Q-value of 8 and 3 at 4.1GHz and 0.9GHz respectively. The performance of the two spirals were tested and verified in LC-VCO and RF bandpass filter circuits, yielding promising results. Ever since, intense research on spiral inductors performance trends, design, optimisation, modelling and Q enhancement has been carried out and reported [12], [35]–[40] in literature. The application of these RF components continued to grow, and today their application is widely extended to higher frequencies including microwave and millimetre wave bands.

2.2 DESIGN MODEL ANALYSIS FOR LOSS COMPENSATION

2.2.1 Conductor Layout Optimisation

Layout optimisation method first appeared in the late 1990s when Craninckx and Steyaert discovered [41] that the largest contributor to high R_s at higher frequencies is at the innermost turns of the spiral. They discovered that the magnetic field induced by the current in the spiral conductor induces an electric field at the inner turns thus generating eddy currents. These currents affect the current distribution in the inner conductor making it inconsistently distributed thus increasing the series resistance. As a result, a new technique in layout optimisation was reported [9] in which the width of the metal trace for each turn is optimised by varying the width from turn-to-turn.

Lopez-Villegas et al. [9] used this technique to design a square spiral inductor in a silicon-based multichip technology complemented with a silicon micromachining post-processing and managed to observe a Q improvement of 60% at a frequency of 3.5 GHz [9]. Recently, Pei et al. [12] applied the same technique on a square spiral with non-uniform strip width and non-uniform winding spacing obtaining an improvement of 42.86% [12]. It is clear that the physical structure and layout of microstrip inductor plays a very important role in Q-factor enhancement. A summary of recent developments on Q-enhancement using the layout optimisation method is presented in Table 2.1.

Table 2.1 – Summary of latest developments in conductor layout optimise inductors

Year	Paper title	Authors	Q_{max}	Refs.
2014	High-Q Characteristics of Variable Width Inductors With Reverse Excitation	Narayana et al.	22.80	[42]
	A Parameterized Cell Design for High-Q , Variable Width and Spacing Spiral Inductors	Manikandan, et al.	22.43	[43]
2013	Analytical Characterization of Variable Width Integrated Spiral Inductors	Passos et al.	-	[44]
2012 and earlier				
	Improving the quality factor of an RF spiral inductor with non-uniform metal width and non-uniform coil spacing	Pei et al.	24.00	[12]

2.2.2 Pattern Ground Shield (PGS)

A. Analysis of PGS inductors

Patterned ground shield (PGS) [7] is one of the various techniques discovered to enhance performance of on-chip spirals for silicon-based RFICs [40]. The technique shorts the electric field to the ground plane. It is patterned with slots orthogonal to the spiral inductor to eliminate the induced current loop by cutting off the current path [7] as indicated in Figure 2.1. These slots are significantly narrower to prevent the vertical electric field from entering the silicon substrate underneath. Shi et al [40] presented a

Q enhancement for PGS inductors at high temperature. Figure 2.1 illustrates the cross-sectional view and circuit model of a PGS spiral fabricated on a 0.35um CMOS process.

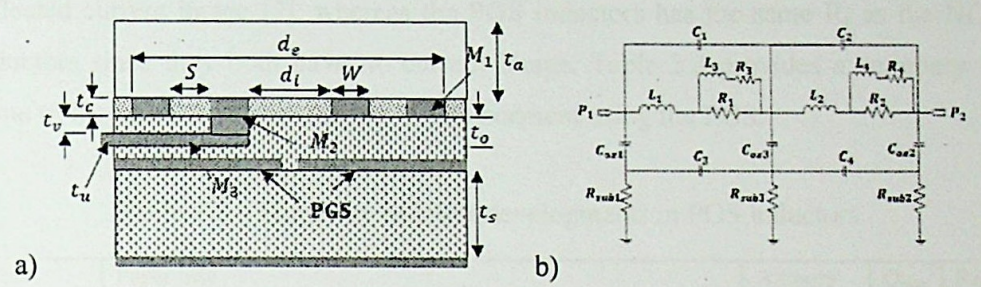


Figure 2.1 – a) Cross-sectional view and b) equivalent lumped-element equivalent circuit model of a PGS on-chip spiral fabricated on a CMOS process

The ohmic loss due to metal coil is represented by R_1 and R_2 whereas R_3 and R_4 represent the losses due to proximity and skin effect of the metal coil. These parameters are temperature dependent, thus vary significantly with temperature change. Other parameters relating to ohmic losses are the R_{subs} which lack temperature dependent properties, especially in a PGS inductor. While these are difficult to extract, they can be easily extracted using the 2-port S-parameter measurements for no-ground shield (NGS) inductors [40]. The minimal spacing in-between the PGS and the spiral means the shunt capacitance of the SiO_2 is given by equation (19), and as a result of the PGS shielding effect, the shunt capacitance in the silicon substrate is almost insignificant as opposed to that of the NGS inductor circuit model.

$$C_{ox} = \frac{C_{ox1} + C_{ox2} + C_{ox3}}{3} \tag{19}$$

Another dissimilarity of a PGS and a NGS inductor is that in a PGS, the section coupling is too high due to a shortened electric return path. This then leads to the introduction of C3 and C4 to reduce the capacitive coupling effects within the SiO_2 layer. A further analysis on the effect of PGS is reported in [45], and a comparison between a solid ground shield (SGS) and PGS is investigated. While PGS may significantly improve Q, SGS on the other hand does not. For SGS, the varying EM

field within the inductor may introduce some eddy currents thus causing reflection on the ground plane which then serve as a counteractive inductor requiring PGS to cut off the current loop [4]. The SGS model therefore has significantly higher R_s due to the reflected current image [7], whereas the PGS inductors has the same R_s as the NGS inductors since they both have no current image. Table 2.2 provides a summary of some of the latest developments on Q enhancement using the PGS.

Table 1.2 – Summary of latest developments in PGS inductors

Year	Paper title	Authors	Q_{max}	Refs.
2015	A Novel WL-Integrated Low-Insertion-Loss Filter with Suspended High- Q Spiral Inductor and Patterned Ground Shields	Zheng et al.	49	[46]
2012 and earlier	On-chip spiral inductors with patterned ground shields for Si-Based RF IC's	Yue et al.	6.76	[7]
	Improving the quality factor of an RF spiral inductor with non-uniform metal width and non-uniform coil spacing	Pei et al.		[12]
	Effect of ground shield of a silicon on-chip spiral inductor	Murata et al.	4.7	[45]

B. Application of PGS inductors

Pokharel and Liu in [47] proposed a low loss, high selective on-chip bandpass filter employing the improved open loop resonator with folded structure and the PGS, achieving a 1.8 dB improvement of insertion loss. Similarly, Liao et al. in [40] demonstrated that a proper PGS can effectively compensate for the degradation of the Q, thus improving the Q of the inductor. The PGS technique effectively reduces the substrate coupling resistance [14]. Tao Zheng et al. [46] used this technique and obtained a high-Q value on a low resistivity silicon wafer.

2.2.3 Differential Excitation

Differential circuits [48] are commonly used to develop monolithic transceiver design due to their robustness and very high noise rejection properties [49]. While these

topologies are used in ICs, they are practically used to excite spiral inductors by connecting the source directly to the two terminals of the spiral inductor [6]. The differential excitation method reduces eddy currents circulation by a significant 30-50% [49] and limit the electrically coupled currents from occurring in the substrate by 50% [48]. A three turn spiral inductor with an outer diameter of 220μm, spiral width of 16 μm, and coil spacing of 2μm was fabricated in a 0.35μm single-poly, four metal CMOS process [3]. This design yielded a differential Q of 3.1, 50% greater than Q of the single-ended excitation at 2.5GHz. A summary of some of the recently reported developments in Q improvement using differential inductors is present in Table 2.3.

Table 2.2 – Summary of latest developments on differentially inductors

Year	Paper title	Authors	Q_{max}	Refs.
2004	Modelling Spiral Inductors in SOS Processes	Kuhn et al.	Q>30@3GHz	[50]
2003	High-Q Differential Inductors for RFIC Design	Reiha et al.	22.7@4GHz	[48]
2002	Differentially Driven Symmetric Microstrip Inductors	Danesh et al.	9.3@2.5GHz	[49]

2.2.4 Negative Resistant (–Rs)

A. Analysis of –Rs Inductor

A negative resistance circuit method reduces substrate loss to improve Q. This circuit produces high percentage increase in Q without reducing the self-resonance frequency (f_{SRF}). This technique is attractive and applicable to high-Q on-chip inductors fabricated on various substrates [51]. On-chip spiral inductors of physical geometry presented in Figure 1.2 of Chapter 1 are represented by a lumped element model of Figure 1.1 (c) with a PGS inductor model in Figure 2.1 (b). The series resistance R_s signifies ohmic losses resulting from metal strip and eddy currents induced in the substrate. While the induction of eddy currents is taken care of by the introduction of PGS described in section 2.2.2, R_s is dominated by the ohmic losses of the conducting strip. This could be eliminated by introduction of by a negative equivalence of R_s as illustrated by Figure 2.2. The negative resistance method is a loss compensation mechanism that introduces a negative resistance of magnitude $-R_s$ to reduce the

dominant ohmic losses in the spiral traces. In this case, the negative resistor is placed in series with $+R_s$ to cancel out or reduce the amount of losses caused by $+R_s$ [52].

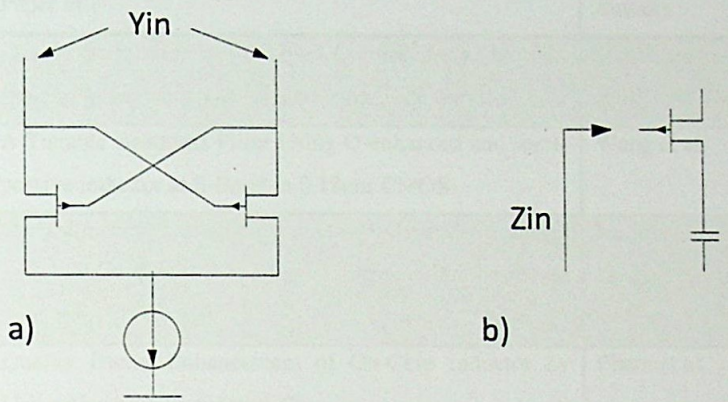


Figure 2.6 – Typical negative resistance/conductance generators

This approach was reported in [52]–[60], stating that the Q is enhanced by using an active negative resistance placed in series to the lossy microstrip inductor. The conservative loss compensation circuit characteristically forms a negative resistance/conductance generator. The dependency of the negative resistance method to frequency means that the negative resistance experience a quadratic decrement with frequency unlike the high frequency characteristics of the metal resistance which increases with frequency as a result of skin effect [52]. Even though the negative conductance in Figure 2.2 (a) is frequency dependent, a frequency dependent negative resistance is introduced in series to the positive resistance of the inductor in cross-connection to the cross-coupled nMOS resistors. The cross-coupled transistors generate negative resistance for sustainable oscillations in the circuit [53]. In addition, [58] states that a tapped-inductor feedback techniques results in a higher-Q by producing a negative feedback. This compensates for the conductor losses related to Q, thus improving the total-Q of the resonating structure. Table 2.4 provides information on latest development in Q-enhancement using the negative resistance technique.

Table 2.3 – Summary of latest developments in spiral inductors with negative feedback

Year	Paper title	Authors	Q_{max}	Refs.
2014	Design and modeling of high-Q variable width and spacing, planar and 3-D stacked spiral inductors	Manikandan et al.	-	[53]
2012 and earlier	A Tunable Bandpass Filter Using Q-enhanced and semi-passive inductor at S-Band in 0.18um CMOS	Wang et al.	-	[58]
	On frequency and quality factor independent tuning possibilities for RF band-pass filters with simulated inductors	Andriesei et al.	-	[55]
	Quality Factor Enhancement of On-Chip Inductor by Using Negative Impedance Circuit	Pham et al.	4.73	[51]
	A 0-dB IL 2140 +/- 30 MHz bandpass filter utilizing Q-enhanced spiral inductors in standard CMOS	Soorapanth et al.	-	[52]

B. Application of $-R_s$-Inductor

Beifort et al reported in [57] a Q-enhanced LC bandpass filter based on the negative resistance method. They investigated and presented a technique for sizing the transistor of the negative resistance based on the approximation of the Q of the novel lossy LC tank, and estimated the effective-Q as in [57] as,

$$Q_{en} = \frac{Q_o}{1-G_{m_o}R_p} \tag{20}$$

where G_{mo} and R_p represents the equivalent trans-conductance of the differential $-R_s$ and the parallel resistance in RLC circuit. Therefore selection of a suitable value of G_{mo} can improve the value of the Q from Q_o to the required Q_{en}. An approximation for G_{mo} calculation is given by the following.

$$G_{mo} = G_m - G_{ds} \tag{21}$$

Here, G_m and G_{ds} are transconductance of the output conductance.

2.3 SUBSTRATE MATERIAL

Substrate material plays a vital role in the overall performance of an integrated circuit. The most important parameters to consider when designing a substrate integrated device are the substrate's resistivity and dielectric loss. This is due to the fact that materials with high resistivity and low dielectric loss tend to enhance performance of resonant circuits [23]. The evolution of substrate technology started from as far as ceramic technology, followed by organic materials and most recently silicon. Lately, there has been more interest in using glass as a substrate for 2.5D/3D application [61]–[63]. Glass proved to provide better electrical performance compared to silicon. Despite it being an insulator, and edged by silicon in terms of conductivity, glass provides reliability performance as a result of possibility to adjust its thermal properties. Glass substrate is reported in [64]–[67]. Several other materials such as low temperature co-fired ceramic (LTCC) are regarded suitable for various applications where metal with excellent conductivity such as gold and silver are used. LTCC have a lower dielectric constant as well as low insertion loss. This makes it an ideal substrate for RF and microwave application. Silicon substrate reported in [7]–[9], [23], [24] is the most commonly used because of its excellent thermal conductivity. Trott and Shorey [68] studied the mechanical properties of glass and silicon, and they reported that a thinned silicon substrate for integrated circuits has become a common process to meet the packaging form factor required by consumer applications [68]. Nonetheless, the thinned silicon substrate is difficult to handle, thus requiring the use of a carrier substrate bonded temporarily as an aid to handling. The procedure for thinning the substrate is illustrated in Figure 2.3.

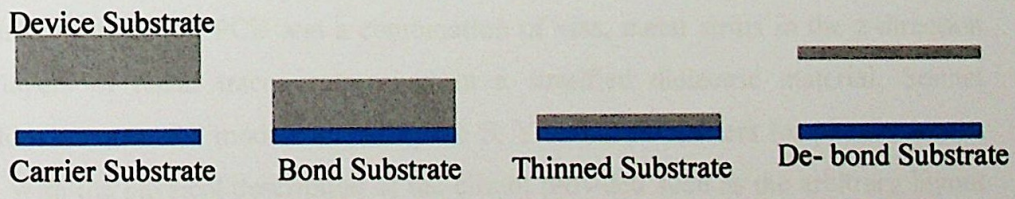


Figure 2.7– Temporary bonded carrier for silicon substrate thinning process [68]

2.4 ELECTROMAGNETIC DESIGN AND SIMULATION TOOLS

One way to evaluate resonant structures is the use of EM simulation tools, used to reproduce the inductor's electrical behaviour under different conditions. Most commonly, the following simulation software have been

2.4.1 High Frequency Structure Simulator (HFSS)

This is a commercial finite element solver for EM structures developed by Ansys [69]. It is a complete solution for modelling arbitrarily shaped 3D EM structures such as antennas, filters and high speed digital circuits. It is a general tool that could be used to design and analyse various EM application [69]. Due to its flexibility and generality, the HFSS simulator is one of the most popular in commercial design environment. It is capable for extraction of parasitic parameters including S, Y and Z-parameters. In addition, the software visualise 3D EM fields and produce SPICE model based on 3D Finite Element Method (FEM) solution of the EM topology under investigation [70]. HFSS has features that offer flexibility in mesh generation and refinement. Such features include the automatic adaptive mesh generator. This makes the simulator more popular and useful for various purposes.

2.4.2 Sonnet Suite™

This is simulation software that uses Method-of-Moment applied directly to Maxwell equations to solve planar problems. The software addresses design challenges involving predominantly 3D planar circuits that include, strip-line, microstrip, coplanar waveguides, PCB and a combination of vias, metal strips in the z-direction and layers of metal traces entrenched in a stratified dielectric material. Sonnet develops accurate RF models including the S, Y and Z-parameters for planar circuits [71]. With the physical description of the circuit provided such as the arbitrary layout and material properties of the conducting metal and substrate material, it is quite easy to use the sonnet tool [72].

2.4.3 CST Microwave Studio®(CST® MWS®)

This is EM simulation software which is considered more precise and efficient for computational solution in the EM design and simulation. It encompasses tools for design and optimisation of devices operational in a wider range of frequencies. The CST software is capable of analysing thermal and mechanical effects of an EM structure [73]. This is an expert tool for 3D EM modelling at higher frequencies, which enable accurate analysis of high frequency devices such as filters, antennas, couplers, planar and multilayer structures [74], signal integrity (SI) and EMC effects [75]. The CST MWS is based on Finite Integration Technique (FIT) and it allows the user to select between the time and frequency domain. As a general purpose simulator, CST competes with HFSS as it gained popularity in the last few years. Nowadays, it is widely used for analysis and design of planar antennas, and detail results are readily available in literature [70].

2.4.4 Optimisers for EM Structures

Selecting a comprehensive optimum of specific electromagnetic (EM) system is a fundamental process for optimising EM systems. Various optimisation algorithms such as stochastic algorithm that include genetic algorithm, simulated annealing, particle swarm etc. are widely used for optimisation process in electrical and electronics engineering. However, most of these algorithms require adequate computational time to find an optimal solution. Parallelisation of the stochastic algorithms is a remedy for computational overhead, but is mostly not sufficient [76]. Effective algorithms need to be built which requires only few model evaluations in order to arrive at the optimal solution. EM optimisation process mostly involves many parameters some of which may be discrete. While handling large number of discrete parameters is a huge task, simulated annealing and genetic algorithms are capable of handling large numbers. Simulated annealing models the hardening of liquid metals to solid metals, while genetic algorithm models evolution and genetic recombination in nature [77]. The two algorithms are programmable, easy and efficient. Over the last few years, GA has gained popularity and has exploded into the research scene with great success, mainly

due to its characteristics that make it a perfect tool that marries relatively well with existing EM analysis techniques, and typically yields results that fulfil the specified requirements in a non-impulsive fashion. A great deal of effort has been expended in expanding the computational maturity of GA optimization in electromagnetics, as well as in extending the domain of applications to include quite creative designs. One distinct focus area in which GA optimization has yielded quite fruitful results are novel pattern synthesis, broadband operation and the development of antennas.[78]

3) CHAPTER THREE

3.1 ELECTROMAGNETIC DESIGN AND ANALYSIS

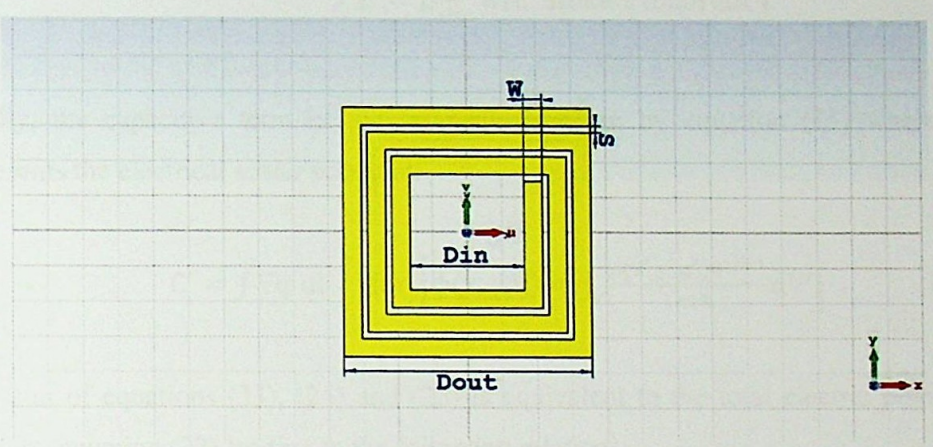


Figure 3.1– Square Spiral Geometry

The formation of the conductive part of this spiral can be analysed using Maxwell's equations. The electric potential on a small length element (*dl*) of a straight segment is given by the product $E_o.dl$, where E_o is the electric field applied. The sum of the product $E_o.dl$ over the straight segment of length *l* is equivalent to the line integral of the product, thus giving the total electric potential of the segment as

$$\Delta V = -\int E_o dl \tag{22}$$

The internal impedance of the segments is given by the line integral of the ratio of current density (J) and segment metal conductivity (σ) as

$$Z' = \int \frac{J}{\sigma} dl \tag{23}$$

The external inductance is represented by equation (24) where $\vec{A}$ represents the magnetic vector potential, k the index running through conductors making the structure, and a term involving Green function [35] denoted R.

$$L' = \int \frac{\partial \vec{A}}{\partial t} dl \quad \text{for} \begin{cases} A(x,y,z) = \mu \int_V \frac{J(x',y',z')e^{-jkR}}{4\pi R} dV' \\ L' = L\frac{dI}{dt} \text{ wrt. Stoke's theorem} \end{cases} \tag{24}$$

Finally, the capacitive term of the segments is given by equation (25) where, ϕ represents the electrical scalar potential.

$$C' = \int \nabla\phi \, dl \quad \text{for} \left\{ \phi(x,y,z) = \int_V \frac{\rho(x',y',z')e^{-jkR}}{4\pi\varepsilon R} dV' \right\} \tag{25}$$

The sum of equations (23), (24) and (25) is equivalent to the total electric potential given by equation (22) leading to the following relation.

$$\int E_o dl - \int \frac{J}{\sigma} dl - \int \frac{\partial \vec{A}}{\partial t} dl - \int \nabla\phi \, dl = 0 \tag{26}$$

The original time-periodic format of the magnetic and electric potentials represented by equations (24) and (25) respectively is practically unrealistic and difficult to compute since the two involve integrating over combined charges and currents in the entire structure including those in the conductor and substrate matter. Practically, the two equations could be rewritten in the form of given by equations (27) and (28) as in [79]. This reduces the integral to just the charge metal segments, thus resulting in a computable format as follows.

$$\phi(r,t) = \frac{1}{4\pi\varepsilon} \sum_k \int_{V_k} G_E(r,r')\rho(r')dV' \tag{27}$$

$$A(r,t) = \frac{\mu}{4\pi} \sum_k \int_{V_k} G_M(r,r')J(r')dV' \tag{28}$$

3.2 CIRCUIT MODELLING AND OPTIMISATION

The geometric layout plays an important role in the inductance and Q of spiral inductor. Thus the initial step in the design is to define the inductor parameters such as

the number of turns (N), width of the coil (W), coil spacing (S), inner and outer diameter. A study [80] developed computational expressions for each parameter in the model as a function of the inductor's geometric values and fabrication process parameter. However, the limitations in validity of some of these expressions owe to the quantitative analysis of an inductor. For example, the calculation of the series resistance (R_s) is based on the DC resistance of the conductor and the skin effect without considering the losses due to proximity effect. Figure 3.2 presents the proposed spiral layout. The width of the inner segment is W and the width of the outer segment is W+ΔW(4N–1) where (ΔW) is the increment in segment width. Equation (29) represents the width of the ith segment and equation (30) signifies the spacing between the ith segment and the $(i+4)^{th}$ segment of the spiral while (ΔS) is the reducing factor.

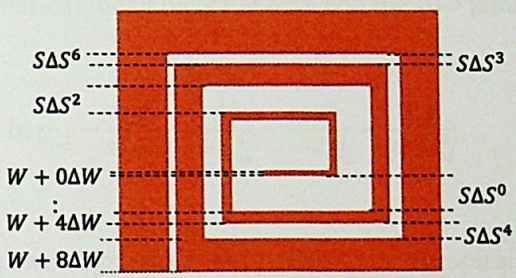


Figure 3.2 – Square spiral with variable segment W&S.

$$W_i = W + \Delta W(i-1) \quad \left\{ \begin{matrix} i \in \mathbb{Z} \\ 1 \le i \le 4N \end{matrix} \right\} \tag{29}$$

$$S_i = S\Delta S^{(i-1)} \quad \left\{ \begin{matrix} i \in \mathbb{Z} \\ 1 \le i \le 4(N-1) \end{matrix} \right\} \tag{30}$$

The series inductance (L_s) is given by

$$L_s = \sum_{i=1}^{4N} L_i + \sum_{i=1}^{4(N-1)} M_i \tag{31}$$

Where L_i is the self-inductance of the ith segment given by

$$L_i = 2l_i \left(\ln \frac{2l_i}{W_i + t_m} + 0.50049 + \frac{W_i + t_m}{3l_i} \right) \tag{32}$$

Where l_i is the length of the i^{th} segment in centimetres (cm), and L_i is the inductance in nano-henrys (nH). Symbol W_i is the width of the ith segment in cm and tm is the metal thickness in cm, constant throughout the spiral turns. Symbol $M_{i,j}$ is the mutual inductance between segments i and j = (i + 4) defined by;

$$M_{i,j} = 2l_i\beta \tag{33}$$

where β is the mutual inductance parameter given by the equation below,

$$\beta = \ln\left[\frac{l_i}{GMD} + \sqrt{1 + \left(\frac{l_i}{GMD}\right)^2}\right] - \sqrt{1 + \left(\frac{l_i}{GMD}\right)^2} + \frac{l_i}{GMD} \tag{34}$$

The GMD defines the geometrical mean distance between the two parallel segments

$$\ln GMD = \ln p_{i,j} - \frac{W_i^2}{12p_{i,j}^2} - \frac{W_i^4}{60p_{i,j}^4} - \frac{W_i^6}{168p_{i,j}^6} - \frac{W_i^8}{360p_{i,j}^8} \cdots \tag{35}$$

Where p is the pitch of the two segments i and j. The Q of the spiral is then given by equation (17) in chapter 1, and the R_s is a frequency-dependent component accounting for the proximity effect and the skin effect on the current flow.

$$R_s = \sum_{i=1}^{4N}\left(\left[\frac{r_s}{W_i} + C\left(\frac{\omega B_i}{2\pi I}W_i\right)^2\right]l_i\right), \qquad \left\{r_s(\omega) = \frac{1}{\sigma\omega\delta(1 - e^{-t/\delta})}\right\} \tag{36}$$

where C is a constant obtained from fitting the simulation results, $r_s(\omega)$ is the metal sheet resistance, B_i is the magnetic field at the i^{th} segment and it consist of three components generated by the i^{th}, $(i + 4)^{th}$and $(i - 4)^{th}$ segment on the i^{th} segment. Symbol ω, σ and δ are the frequency in radians, conductivity and skin depth of the metal segment respectively. Lastly, ρ and μ are the electrical resistivity and permeability of the conductor respectively. δ is given by

$$\delta = \sqrt{(2\rho/\omega\mu)} \tag{37}$$

3.3 ANALYTIC MODELLING AND PROXIMITY EFFECT

The non-uniform current distribution in segments of spiral in Figure 3.2 is typically due to the skin effect which exists at all frequencies. However, the effect is only considerable at lower frequencies whereas at higher frequencies it is overshadowed by the proximity effect. This effect is a result of magnetic fields from adjacent conductors as shown in Figure 3.3(a) and has a greater impact than skin effect on the total-Q of the coil in a wide-ranging bandwidth towards the mm-wave range [48]. Also known as the current crowding effect, proximity effect is a well-known phenomenon responsible for increasing the effective resistance and reducing Q in a multi-turn spiral [81]. While it is negligible in conductors carrying current in opposite direction, it is significant in conductors carrying current in the same direction and is modelled by treating the two adjacent conductors as one conductor of effective W_{eff} for $W \gg S$ [82] as illustrated in Figure 3.3(a). While increasing W drops the ohmic losses by a 1/W at lower frequencies, the decline is much slower at higher frequencies due to the skin effect. Considering the rectangular cross-section in Figure 3.3(b) of the i^{th} segement, and assuming a current flow in the z-direction, the basic equations for the electric field and magnetic flux can be deduced. This is possible since the electric field strength and magnetic flux density are directly proportional to the current density(J). The curent density is in the z-direction, thus the electric field strength has only the z-component E_z satisfying equation (38) under harmonic excitation and steady state condition [83].

$$\frac{\partial^2 E_z}{\partial x^2} + \frac{\partial^2 E_z}{\partial y^2} - k^2 E_z = 0 \tag{38}$$

Where $k = \sqrt{k_x^2 + k_y^2}$ and k_x and k_y are complex wave constants. The solution to the partial differential equation (38) is then given by,

$$E_z(x, y) = E_{z0} \cosh(k_x x) \cosh(k_y y) \tag{39}$$

Therefore, with the help of Maxwell's equation and application of Faraday's law, the following magnetic flux components are determined.

$$B_x(x,y) = B_{x0}\sinh(k_x x)\cosh(k_y y) \tag{40}$$

$$B_y(x,y) = B_{y0}\cosh(k_x x)\sinh(k_y y) \tag{41}$$

$$B_z(x,y) = 0 \tag{42}$$

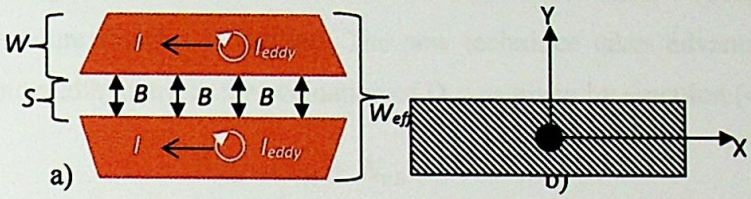


Figure 3.3 – (a) Parallel current carrying spiral segments modelling proximity effect (b) segment cross-sectional view

A demonstration in Figure 3.4 shows the distribution of electrically induced currents resulting in a significantly low magnetic field. This can be verified at lower frequencies with the magnetic (∇) and electric ($\nabla\phi$) vector potentials noting that $\nabla \times \nabla\phi \equiv 0$ [84].

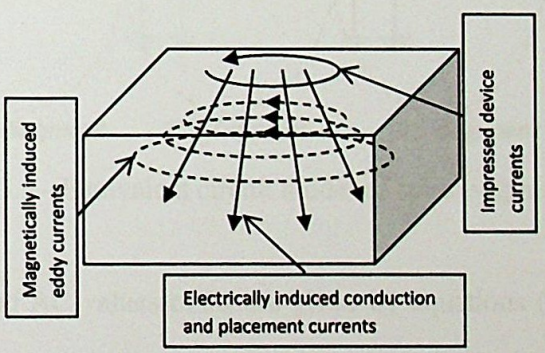


Figure 3.4 - Schematic representation of electrically and magnetically induced currents

Typically, spirals are interconnects of various metal segments cascaded together to form a minimum four sided coil. The four sided coil is a square spiral which consist of four segments per turn as in Figures 3.1 and 3.2. Accordingly, the square spiral of N

turns has 4N segments, and each segment has two branches, one relating to L_s and R_s. The second branch is associated to the substrate impedance. Assuming a dense capacitive coupling impedance matrix, an additional branch of lossy capacitors is added from one segment to another. This increases the total number of branches by $(s+1)(s+2)/2$ where (s) represents the number of segments. These branches can be seen in the lumped element model in Figure 3.5. The elementary structure for supporting all segments characterization is denoted by the scalar matrix equations (46) and (47). With regard to the π-model inductance (L_s) of the whole structure, a new evaluation procedure for D_{out} is devised. The new technique takes advantage of the spiral length and width matrices for evaluation of D_{out} as given by equation (43).

$$D_{out} = l_{n4} + W_{n5} \tag{43}$$

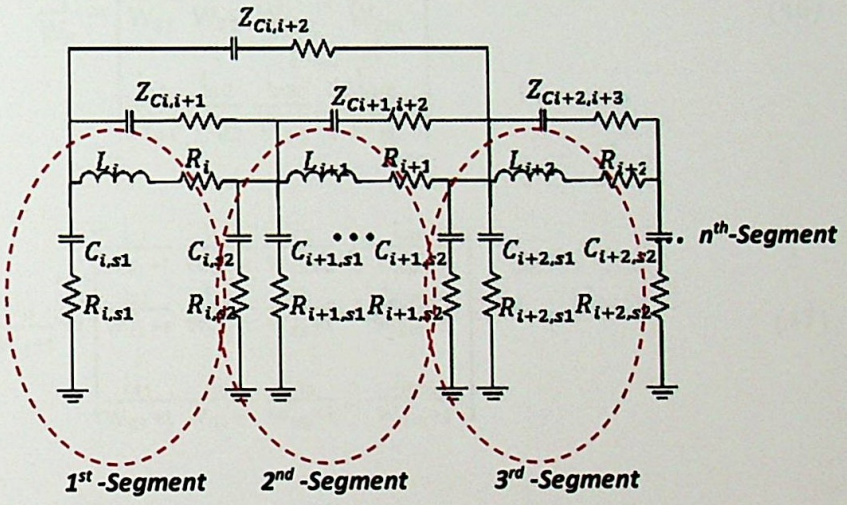


Figure 3.5 - Equivalent circuit model of spiral segments

In addition, the DC and AC values of R_s are given by equations (44) and (45) as in [85].

$$R_{dc} = \frac{1}{\sigma t}\sum_{i=1}^{N}\sum_{j=1}^{5}\frac{l_{ij}}{W_{ij}} \tag{44}$$

$$R_{ac} = \frac{k}{2\sigma\delta}\sum_{i=1}^{N}\sum_{j=1}^{5}\frac{l_{ij}}{W_{ij}+t} \tag{45}$$

Where l_{ij} and W_{ij} are the scalar quantities of matrices describing the length and width of each segment. Therefore a scalar matrix containing all information regarding the geometry of each segment with regard to the DC and AC resistance is generated and described by equations (46) and (47) respectively [85] where n represent the nth turn and m represent the mth segment.

$$\frac{l_{ij}}{W_{ij}} = \begin{bmatrix} \frac{l_{11}}{W_{11}} & \frac{l_{12}}{W_{12}} & \frac{l_{13}}{W_{13}} & \cdots & \frac{l_{1m}}{W_{1m}} \\ \frac{l_{21}}{W_{21}} & \frac{l_{22}}{W_{22}} & \frac{l_{23}}{W_{23}} & \cdots & \frac{l_{2m}}{W_{2m}} \\ \vdots & \vdots & \vdots & & \vdots \\ \frac{l_{n1}}{W_{n1}} & \frac{l_{n2}}{W_{n2}} & \frac{l_{n3}}{W_{n3}} & \cdots & \frac{l_{nm}}{W_{nm}} \end{bmatrix} \tag{46}$$

$$\frac{l_{ij}}{W_{ij}+t} = \begin{bmatrix} \frac{l_{11}}{W_{11}+t} & \frac{l_{12}}{W_{12}+t} & \frac{l_{13}}{W_{13}+t} & \cdots & \frac{l_{1m}}{W_{1m}+t} \\ \frac{l_{21}}{W_{21}+t} & \frac{l_{22}}{W_{22}+t} & \frac{l_{23}}{W_{23}+t} & \cdots & \frac{l_{24=m}}{W_{2m}+t} \\ \vdots & \vdots & \vdots & & \vdots \\ \frac{l_{n1}}{W_{n1}+t} & \frac{l_{n2}}{W_{n2}+t} & \frac{l_{n3}}{W_{n3}+t} & \cdots & \frac{l_{nm}}{W_{nm}+t} \end{bmatrix} \tag{47}$$

This technique alters the substrate modelling expressions for C_{ox}, C_{si} and R_{si} as in equations (48) – (50) for which a supplementary matrix expressing the area of each segment is considered since these parameters are proportional to the area covered by each segment [85].

$$C_{ox} = \frac{\varepsilon_{ox}}{2t_{ox}}\sum_{i=1}^{N}\sum_{j=1}^{5} l_{ij}W_{ij} \tag{48}$$

$$C_{si} = \frac{C_{sub}}{2}\sum_{i=1}^{N}\sum_{j=1}^{5} l_{ij}W_{ij} \tag{49}$$

$$R_{si} = \frac{2}{G_{sub}} \sum_{i=1}^{N} \sum_{j=1}^{5} \frac{1}{l_{ij} W_{ij}} \qquad (50)$$

3.4 NUMERICAL ANALYSIS AND RESULTS

Two spirals, one with a variable metal width increasing from inner turn to the outer turn and the other with a variable metal width increasing from inner segment to outer segment were investigated. Using equation (2), a numerical evaluation of the spirals Q was evaluated and presented by Figure 3.6. The figure present data calculated from spiral inductors with a variable-turn-width (VTW) configuration and a variable-segment-width (VSW) configuration respectively. The data show that each spiral has the highest Q peak at around 2GHz as per design specification, with the former having a value of 44.15 at 2.15 GHz and the latter a Q-value of 49.28 at exactly 2GHz.

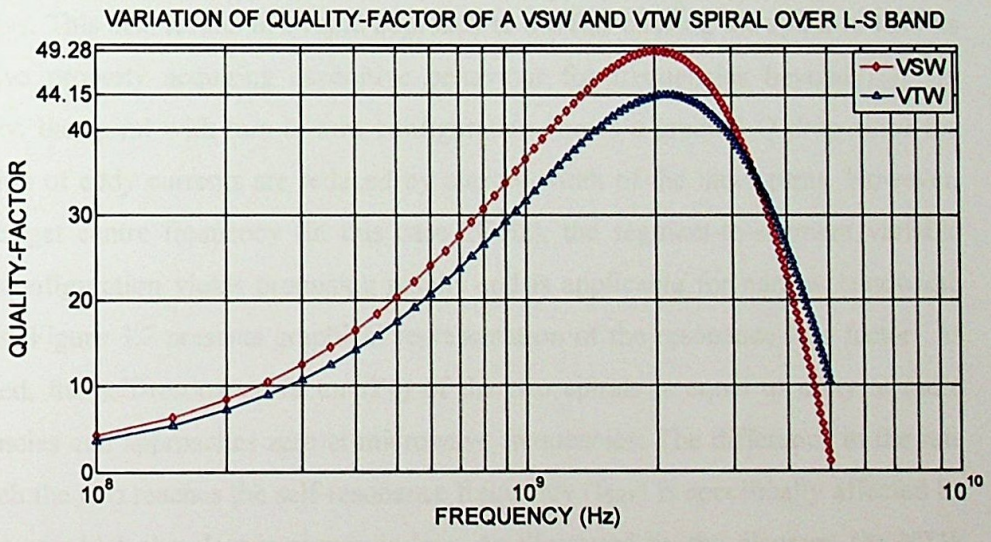


Figure 3.6 – Graph of Q versus frequency of VTW and VSW spirals

Within the L-S band, the turn-to-turn variable width spiral configuration yields Q-values ranging from 31.63 at the lowest frequency (1GHz) of the L-S band to 44.15 at 2.15GHz, and 26.13 at the highest frequency of the L-S band (4GHz). On the other hand, the new segment-to-segment variable width configuration yields Q-values ranging from 36.44 at 1GHz to the highest Q-peak of 49.28 at 2GHz, and down to 22.7

at 4GHz. The steep in energy loss after the resonance frequency is due to the rapid increase in parasitic capacitive effects as the frequency increases. The numeric Q-results at various frequency points in the L-S band are given in Table 3.1 below as calculated from the graphical results in Figure 3.6.

Table 3.1 – Q-value comparison at selected frequencies within the L-S Band

	Q@1GHz	Q@1.5GHz	Q@2GHz	Q@2.5GHz	Q@3GHz	Q@3.5GHz	Q@4GHz
VTW	31.63	40.5	44	43.14	39.18	33.23	26.13
VSW	36.44	46.15	49.28	47.05	41.03	32.58	22.7

The increasing electric fields due to capacitive effect resulting from wider spiral segment widths closer to the centre of the inductor leads to generation of eddy currents at the centre diminishing the overall performance of the inductor as frequency increases. This also results in a rapid approach to the f_{SRF} causing the spiral to lose its inductive property acquiring capacitive behaviour for frequencies beyond f_{SRF}. In contrary, the spiral with turn-to-turn configuration shows a gradual Q drop since the induction of eddy currents are reduced by narrow width of the inner turns. However, for a target centre frequency (in this case 2GHz), the segment-to-segment variable width configuration yields promising results and is applicable for narrow bandwidth devices. Figure 3.7 presents graphical representation of the resonance loss factor. As expected, the self-resonance factor (F_R) of the two spirals is equal to unity at radio frequencies and approaches zero at microwave frequencies. The difference in the rate at which the two reaches the self-resonance frequency (f_{SRF}) is specifically affected by the rate at which the electric energy is lost. As illustrated by the diagram, the VTW configuration has a higher f_{SRF} compared to the VSW configuration due to wider strip widths closer to the centre.

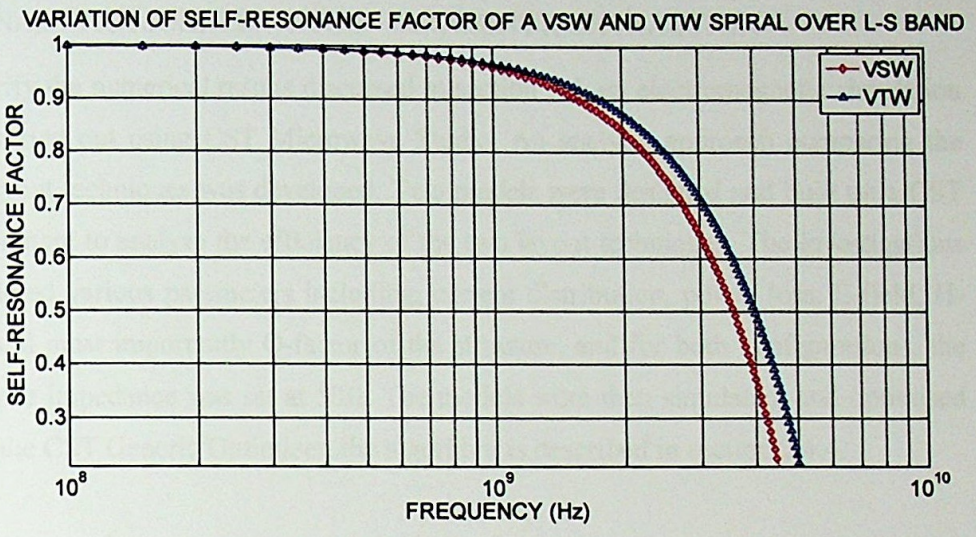


Figure 3.7 – Self-resonance factor of a VTW and VSW structure

Likewise, the effect of the substrate-loss factor was investigated as the frequency increases. But unlike the F_R, the F_S is similar for both types of spiral regardless of metal layout structure. This is because the F_S is dependent on substrate parameters only, and for as long as the same substrate material has been used, the parameters remain the same. For that reason, an illustration in Figure 3.8 shows a single graph indicating that the F_S of both spirals is measurable and equal across similar points.

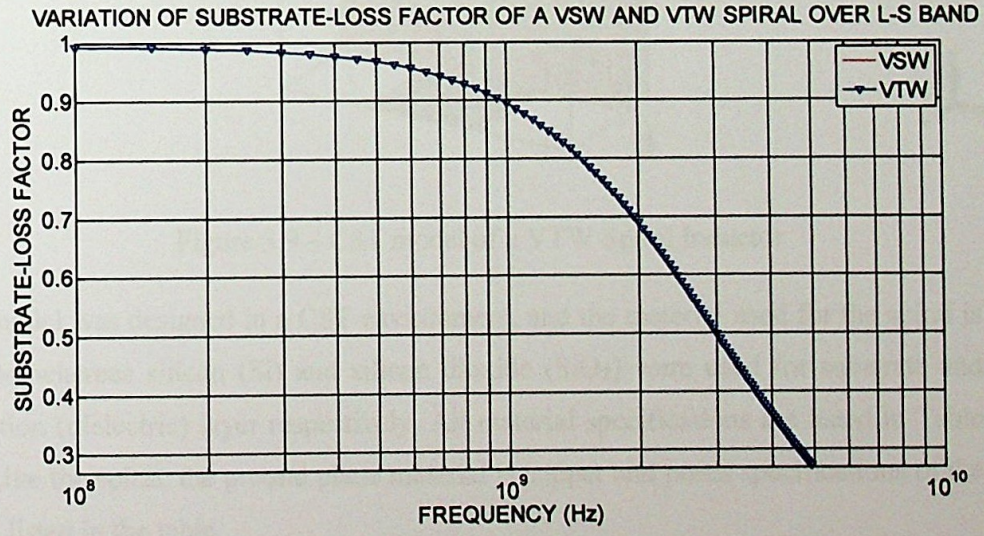


Figure 3.8 – Substrate loss factor of a VTW and VSW structure

3.5 ANALYTIC MODELLING AND PARAMETER EXTRACTION

To verify the numerical results discussed in section 3.4, an electromagnetic simulation was carried out using CST Microwave Studio. An analytic approach comparing the two layout techniques was developed. Two models were designed and built on a CST environment to analyze the efficiency of the two layout techniques. The investigations considered various parameters including, current distribution, power loss, E-field, H-field and most importantly Q-factor of the structure, and for both configurations, the reference impedance was set at 50Ω. The models were then simulated, and optimised using the CST Generic Optimizer, the algorithm is described in section 2.4.4.

3.6 ELECTROMAGNETIC SIMULATION

3.6.1 A Variable Turn Width (VTW) Spiral Inductor

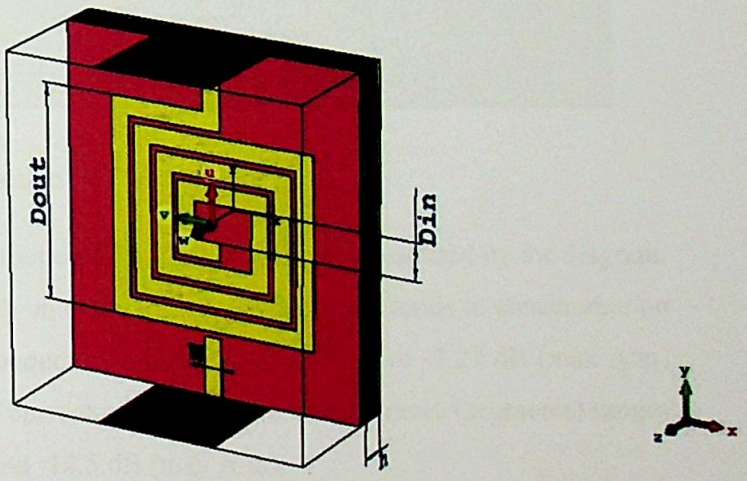


Figure 3.9 – CST model of a VTW Spiral Inductor

The model was designed in a CST environment, and the material used for the spiral is copper, whereas silicon (Si) and silicon dioxide (SiO_2) were used for substrate and oxidation (dielectric) layer respectively. All material specifications are listed in Table 3.2. Like the spiral, the ground plane material is copper and poses specifications of the spiral listed in the table.

Table 3.2 – Material specifications

Substrate	Spiral	Dielectric
Silicon (lossy) Type: Normal Epsilon 11.9 Mue:1 El. Cond:0.00025 [S/m] Rho:2330 [kg/m^3] Therm.cond:148 [W/K/m] Heat cap. 0.7 [kJ/K/kg] Diffusivity: 9.07419e-005[m^2/s] Young's Mod.112 [kN/mm^2] Poiss. Ratio 0.28 Thermal Exp. 5.1 [1e-6/K]	Copper (annealed) Lossy metal Mue:1 El. cond. 5.8e+007 [S/m] Rho 8930 [kg/m^3] Therm. cond. 401 [W/K/m] Heat cap. 0.39 [kJ/K/kg] Diffusivity 0.000115141 [m^2/s] Young's Mod. 120 [kN/mm^2] Poiss. Ratio 0.33 Thermal Exp. 17 [1e-6/K]	Silicon Dioxide (optical) Type: Normal Disp. eps. Nth order model, N=4 (fit) Mue:1

A. Surface Currents distribution (VTW)

Figure 3.10 shows current distribution on a VTW model. As illustrated by the diagram, the proximity effect is very high on every turn, and the current tends to concentrate on the edges and corners of the conductor reaching a value of up to -7.27 dB (max A/m) at the edges. The magnitude of current in the middle of metal traces (segments) ranges between -21.8 dB (max A/m) and -14.5 dB (max A/m).

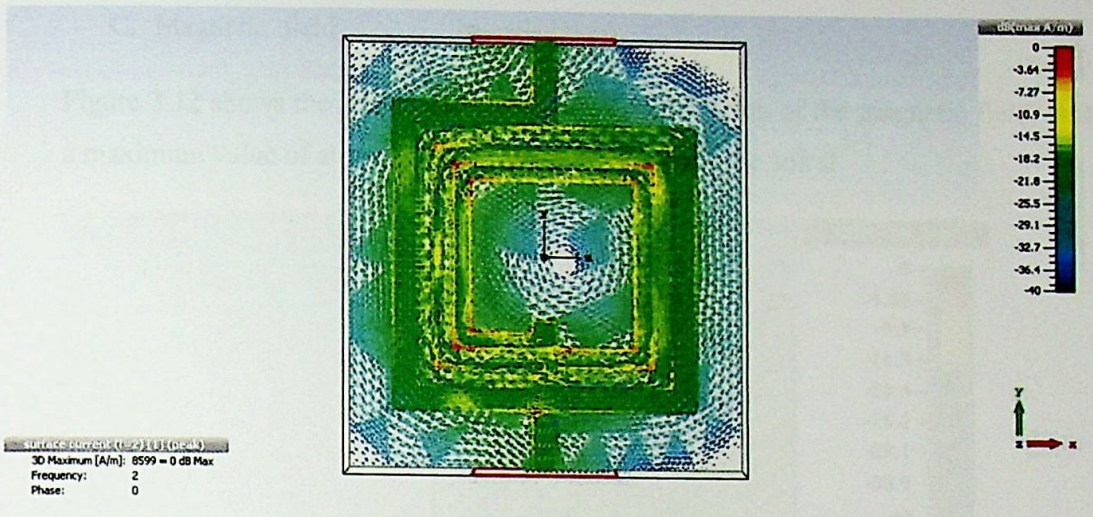


Figure 3.80 – Surface Current Distribution in a VTW model

B. Electric field

Figure 3.11 illustrates the intensity of electric field induced around the resonator. The electric field is significant with a value of up to -24.2 dB (max V/m).

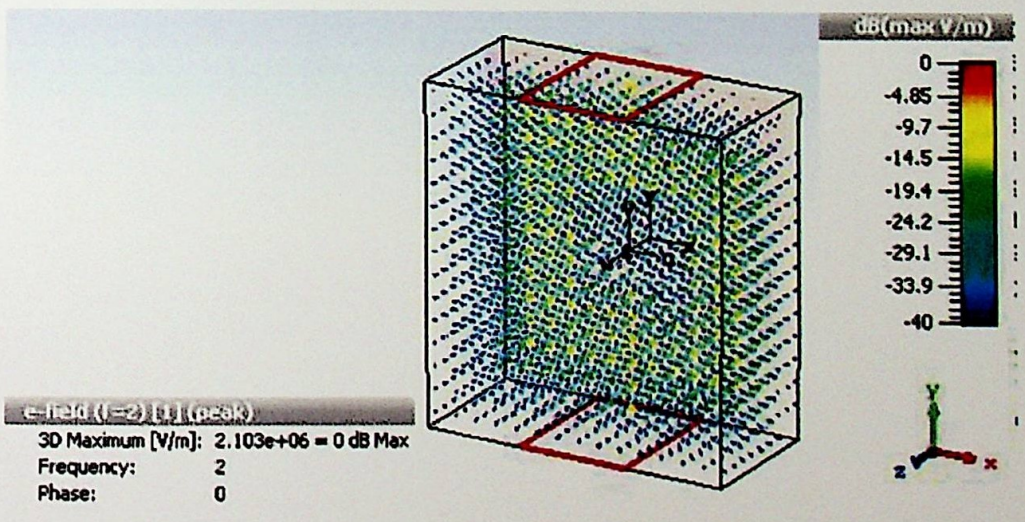


Figure 3.11 – Electric Field Distribution in a VTW model

C. Magnetic field

Figure 3.12 shows the magnitude and area of concentration of the magnetic field, with a maximum value of around -9.7 dB (max A/m) around the spiral.

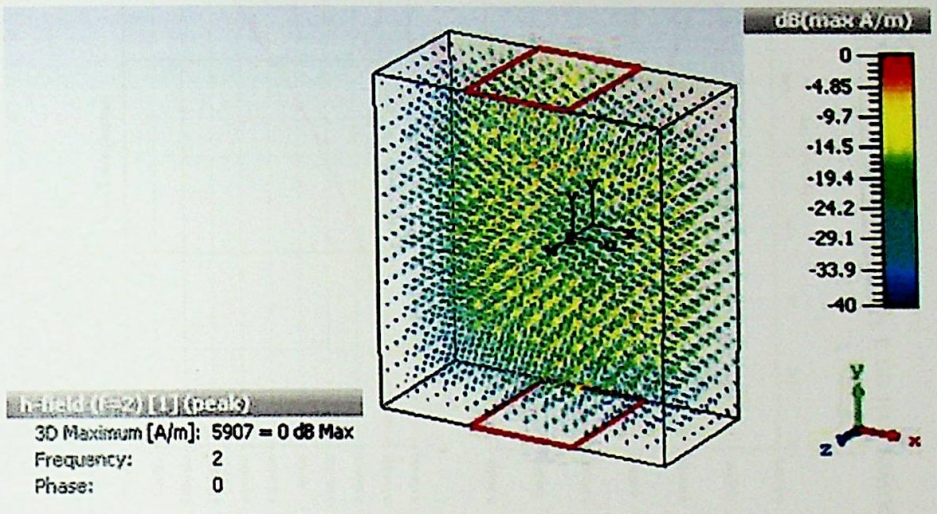


Figure 3.92 – Magnetic Field Distribution in a VTW model

D. Power developed and Power lost (VTW)

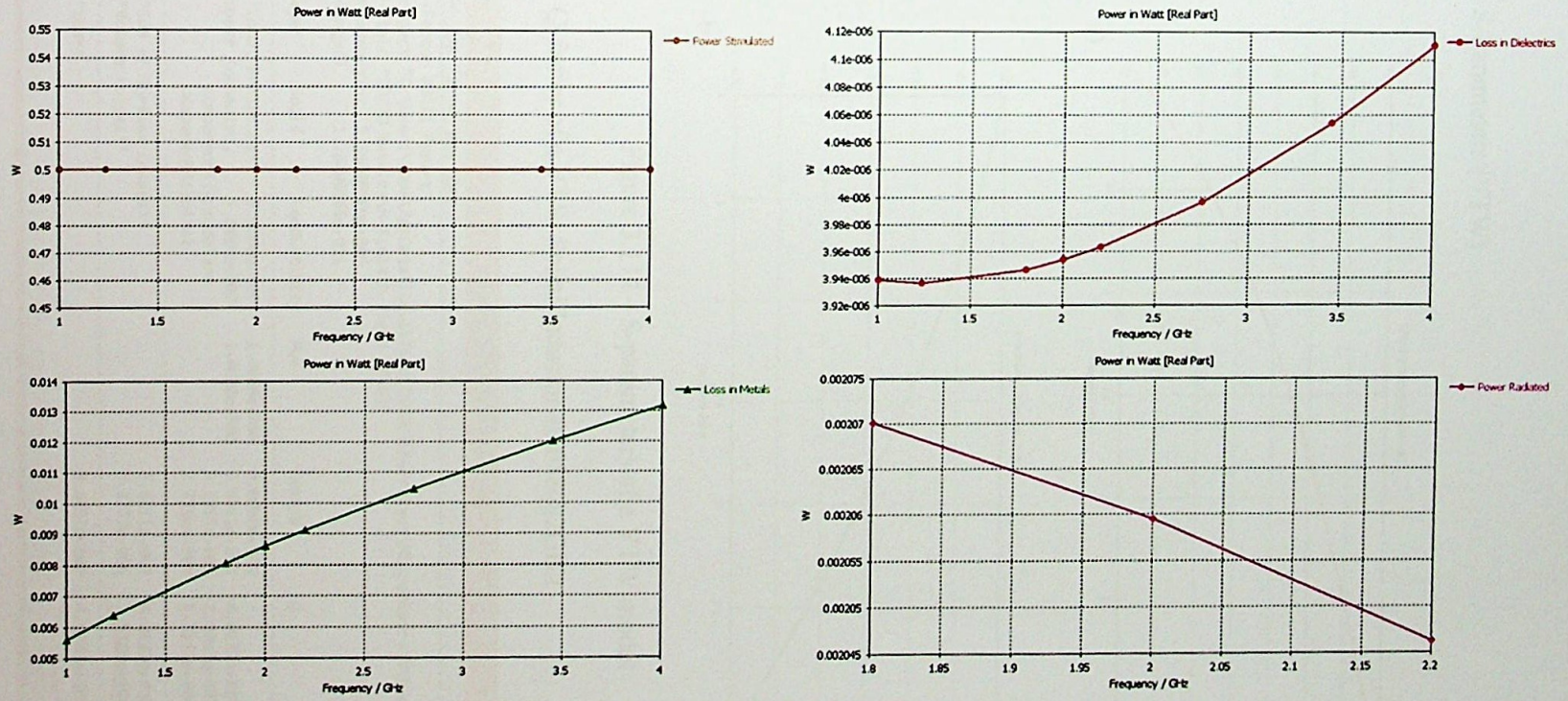
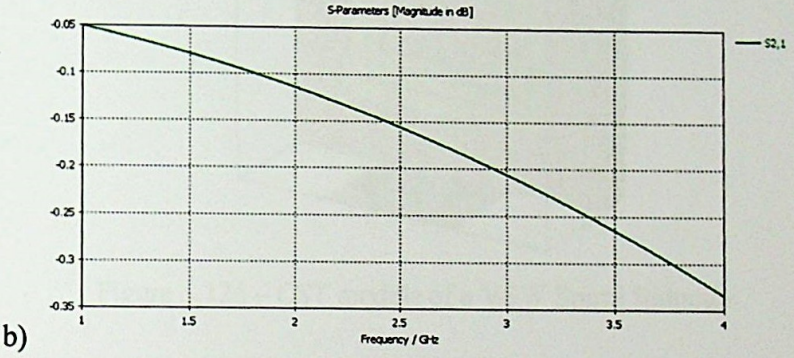


Figure 3.103 – Power simulated vs. power lost on a VTW model

E. S-Parameters (VTW)



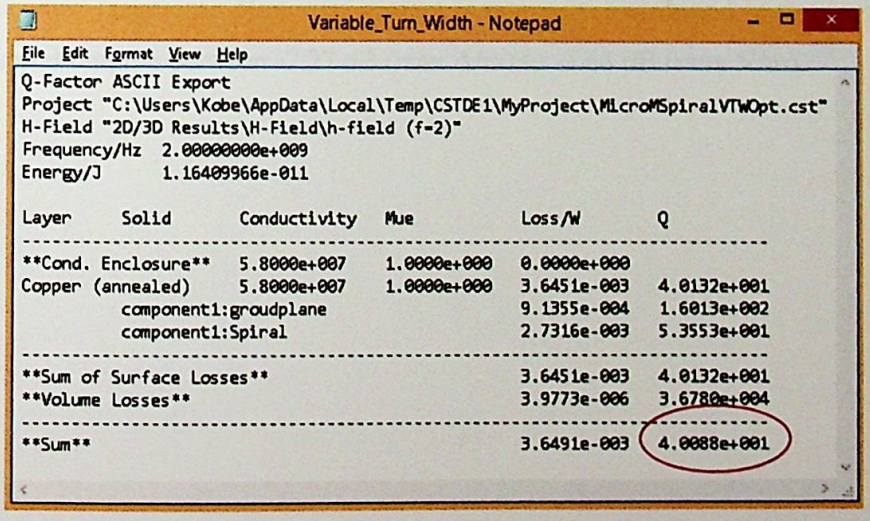
a)



b)

Figure 3.114 – S-parameters of a VTW model

F. Q-factor of a VTW Spiral Inductor 40.088@2GHz



Variable_Turn_Width - Notepad

File Edit Format View Help

```
Q-Factor ASCII Export
Project "C:\Users\Kobe\AppData\Local\Temp\CSTDE1\MyProject\MicroMSpiralVTWOpt.cst"
H-Field "2D/3D Results\H-Field\h-field (f=2)"
Frequency/Hz  2.00000000e+009
Energy/J      1.16409966e-011

Layer      Solid        Conductivity   Mue           Loss/W        Q
-------------------------------------------------------------------------
**Cond. Enclosure**   5.8000e+007    1.0000e+000   0.0000e+000
Copper (annealed)     5.8000e+007    1.0000e+000   3.6451e-003   4.0132e+001
          component1:groudplane                     9.1355e-004   1.6013e+002
          component1:Spiral                         2.7316e-003   5.3553e+001
-------------------------------------------------------------------------
**Sum of Surface Losses**                           3.6451e-003   4.0132e+001
**Volume Losses**                                   3.9773e-006   3.6780e+004
-------------------------------------------------------------------------
**Sum**                                             3.6491e-003   4.0088e+001
```

Figure 3.15 – Quality-factor ASCII Export file from CST MWS (VTW model)

3.6.2 A Variable Segment Width (VSW) Spiral Inductor

The material used to model the VSW model in Figure 3.16 is listed in Table 3.2. For fair comparison, the two models, VTW and VSW were modelled in the same environment and with the same materials.

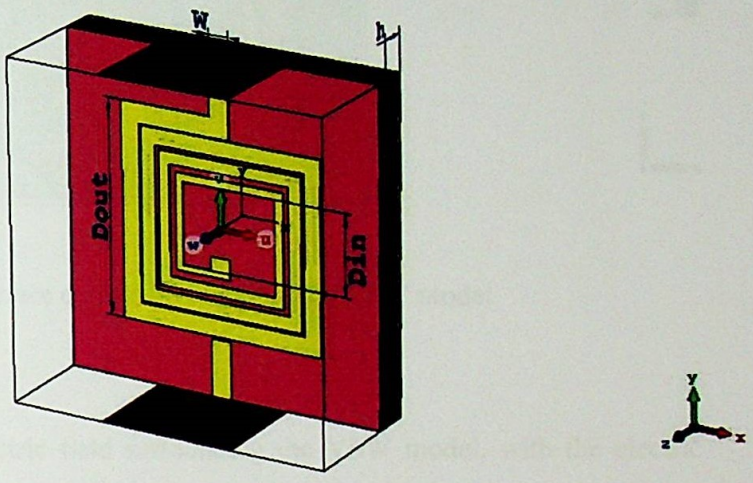


Figure 3.126 – CST models of a VSW Spiral Inductor

A. Surface Currents distribution (VSW)

Figure 3.17 illustrates surface current distribution on a VSW model. Current is evenly distributed with a max value of -7.27 dB (max A/m) measure across the width of each metal trace (segment). However, current is unevenly distributed in the inner turns of the spiral ranging between -7.27 dB (max A/m) to -3.64 dB (max V/m).

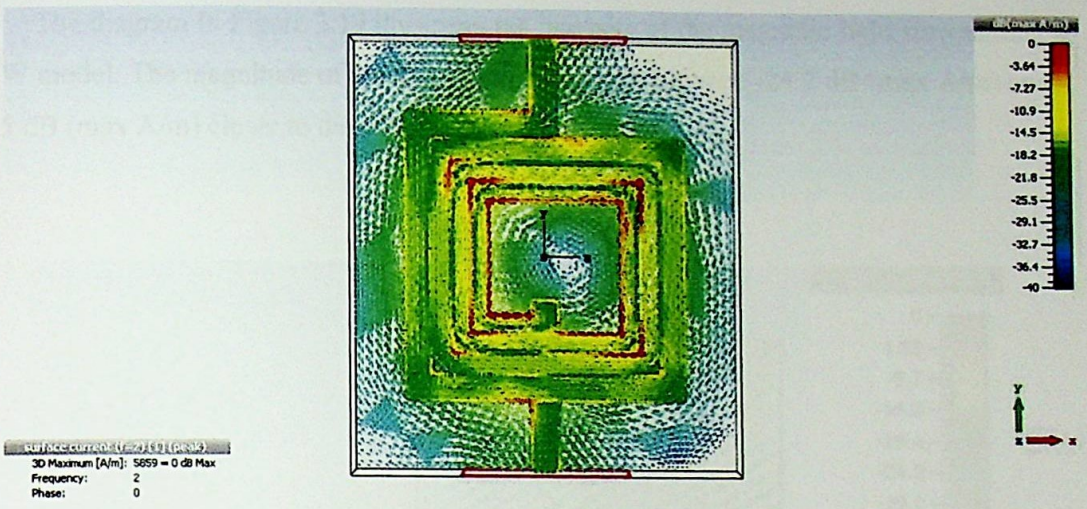


Figure 3.17 – Surface current distribution in a VSW model

B. Electric field

Figure 3.18 shows low electric field surrounding the VSW model, with the electric field ranging between -40 dB (max A/m) and -23.9 dB (max A/m).

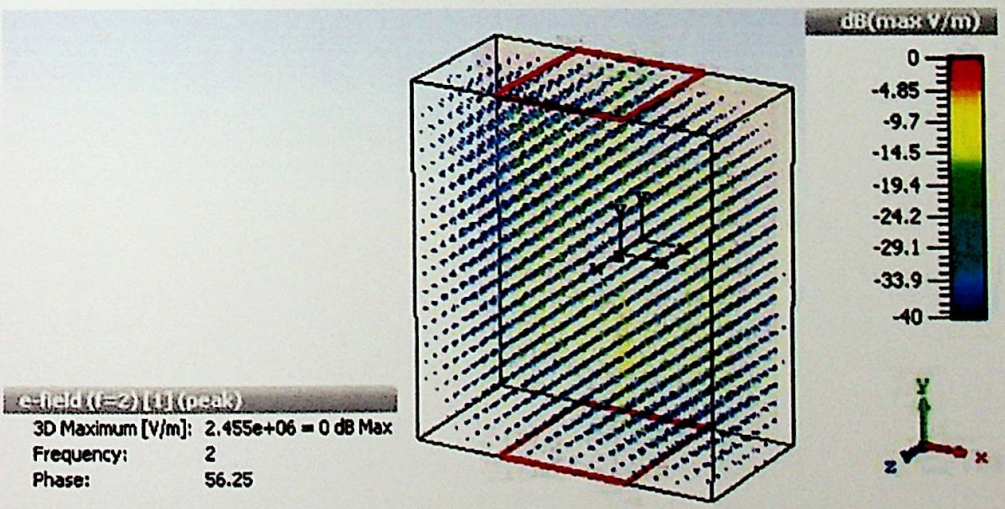


Figure 3.18 – Electric Field Distribution on a VSW model

C. Magnetic field

The diagram in Figure 3.19 illustrates the intensity of the magnetic field surrounding a VSW model. The magnitude of the magnetic field ranges between -24.2 dB (max A/m) and -14.5 dB (max A/m) closer to the metal traces (segments).

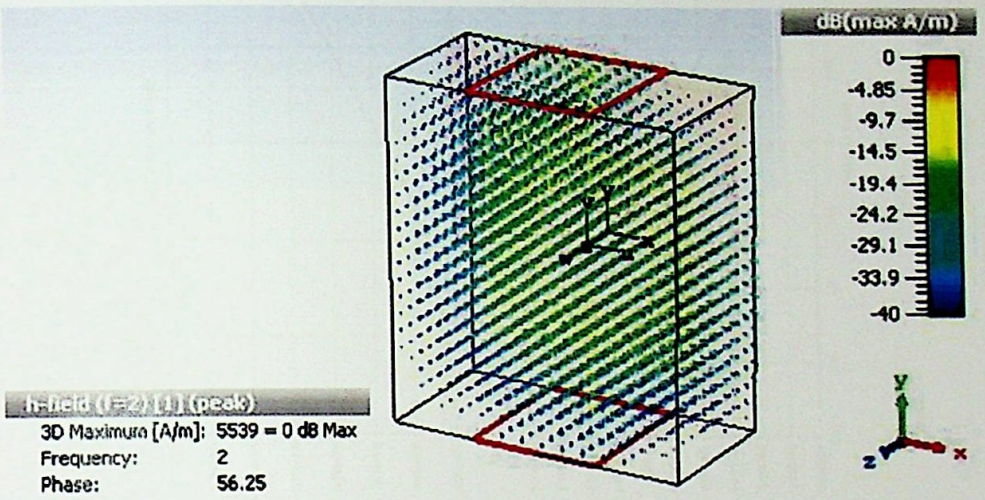


Figure 3.19 – Magnetic Field Distribution on a VSW model

D. Power developed and Power lost (VSW)

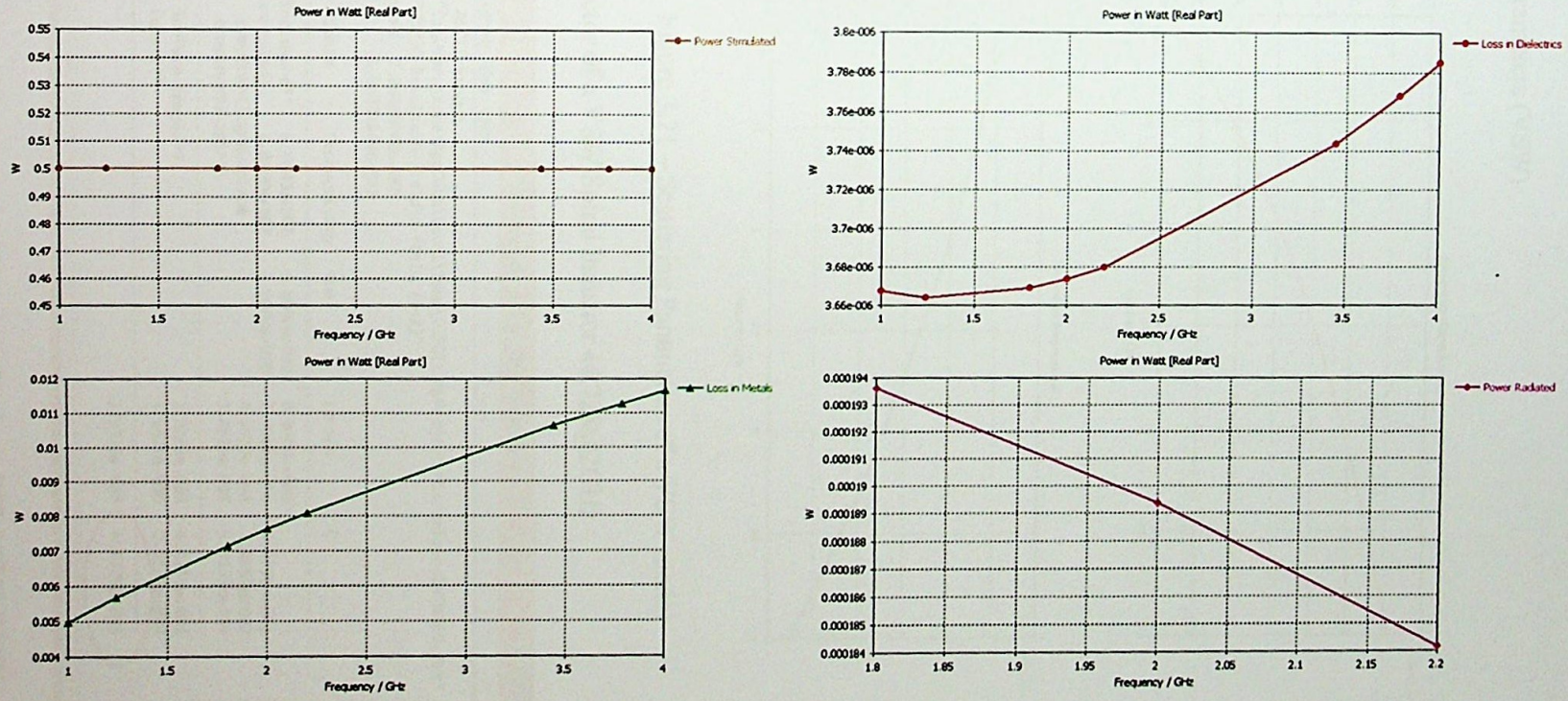


Figure 3.20 – Power simulated vs. power lost on a VSW model

E. S-Parameters (VSW)

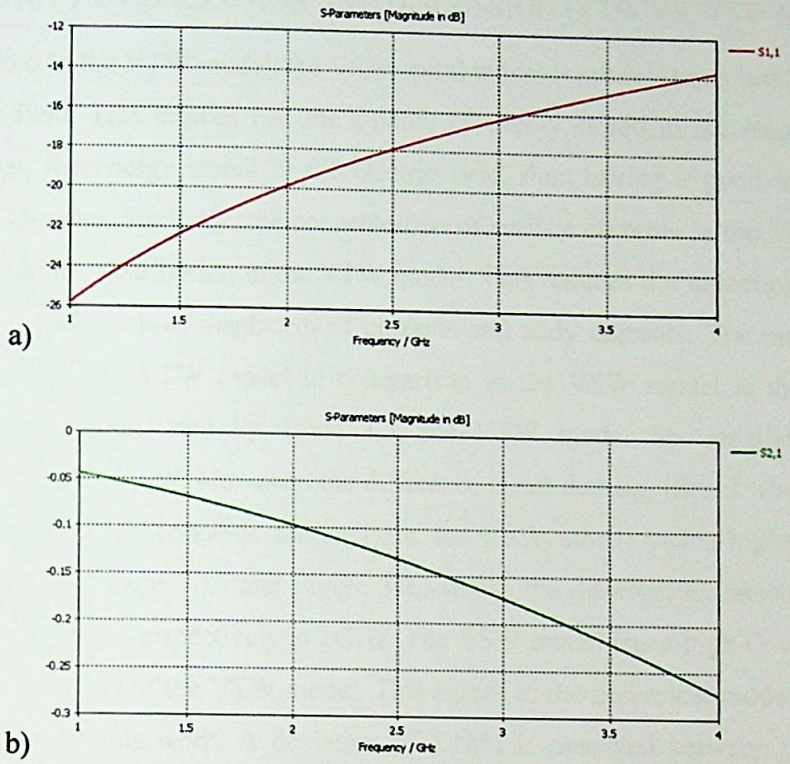


Figure 3.21 – Scattering Parameters of a VSW model

F. Q-Factor of a VSW Spiral Inductor 44.728@2GHz

Variable_Segment_Width - Notepad

File Edit Format View Help

```
Q-Factor ASCII Export
Project "C:\Users\Kobe\AppData\Local\Temp\CSTDE1\MyProject\MicroMSpiralVSWOpt.cst"
H-Field "2D/3D Results\H-Field\h-field (f=2)"
Frequency/Hz  2.00000000e+009
Energy/J      1.04391669e-011

Layer     Solid       Conductivity   Mue          Loss/W       Q
-------------------------------------------------------------------------
**Cond. Enclosure**   5.8000e+007    1.0000e+000  0.0000e+000
Copper (annealed)     5.8000e+007    1.0000e+000  2.9283e-003  4.4799e+001
          component1:groudplane                   4.5932e-004  2.8560e+002
          component1:Spiral                       2.4689e-003  5.3133e+001
-------------------------------------------------------------------------
**Sum of Surface Losses**                         2.9283e-003  4.4799e+001
**Volume Losses**                                 4.6621e-006  2.8138e+004
-------------------------------------------------------------------------
**Sum**                                           2.9329e-003  4.4728e+001
```

Figure 3.22 – Quality-factor ASCII Export file from CST MWS (VSW model)

3.7 ANALYTIC CONCLUSION AND DISCUSSION (VTW VS. VSW MODEL)

Compared to the VTW model, the VSW spiral inductor model stores less energy in the electric field. This implies that the amount of energy stored in the magnetic field is high than the energy stored in the electric field, thus having a good impact on the overall Q-value. Similarly, the concentration of surface currents in the VSW model is better than the distribution in the VTW model. This reduces the induction of substrate related losses, such as displacement currents and eddy currents. The only advantage possessed by the VTW model in comparison to the VSW model is the size of the structure. As illustrated by Table 3.3, the VTW model has smaller dimensions compared to the VSW. However, the difference is not that significant where size is not a big problem. To conclude the analysis, the VSW model yields higher-Q than the VTW model. Figure 3.15 and Figure 3.22 shows the different extracted Q-values of the two structures respectively at 2GHz. The VSW model has a high-Q value of about 11.57 % to the Q of the VTW model. This agrees to the numerical model discussed in section 3.4 of this work. A deviation of 5.18% is observed between the numerical value and the practical value. The reason for deviation is probably due to the losses induced in the practical modelling of which the numerical modelling does not account for, such as the radiation and thermal emissions.

Table 3.3 – Dimensions of the two models (VTW vs. VSW model)

	W_{min}	W_{max}	ΔW	S_{min}	S_{max}	ΔS	Dout	H	W_{sub}	L_{sub}	Q_{max}
VTW	10.35	24.46	4.70	3.93	8.32	2.08	362	39.75	478.12	509.37	40.088
VSW	10.75	29.71	1.35	2.19	12.55	1.32	349	42.37	482.81	526.56	44.728

A comparison of powers in Figures 3.13 and 3.20 shows that for an equal amount of power simulated on each model, the VSW model has lower radiation as compared to the VTW model. Also, the power lost in metal and dielectric is lower in the VSW model. This shows efficiency of the new layout technique as compared to the previous technique.

3.7.1 Comparison with similar existing work

A comparison of this work to other existing works of similar structures and objectives is illustrated in Table 3.4. it is clear from the comparison that the current work yields better results in terms of Q-factor than the previously used methods.

Table 3.4 – comparison of current results with existing similar work

Year/Ref.	Title/Description	Q-Improvement compared to conventional design
2017/(This work)	Variation of spiral width from one segment to another with non-uniform coil spacing	**38.9%**
2015/[86]	Layout Optimized Non-Uniform Series-Parallel Inductors for High Inductance Density and Quality Factor	30%
2014/[53]	Design and modeling of high-Q variable width and spacing, planar and 3-D stacked spiral inductors	20%
2013/[85]	Variation of spiral width from one segment to another with non-uniform coil spacing	30%

3.8 PUBLICATIONS

O.B. Kobe et al., "A review on quality factor enhanced on-chip microwave planar resonators, Eng. Sci. Tech., Int. J. (2016), Elsevier". PUBLISHED:@ http://dx.doi.org/10.1016/j.jestch.2016.09.024

O.B. Kobe et al. "Modelling high-Q square spiral with variable segment width and spacing, 2016 IEEE Radio and Antenna days of the Indian Ocean (RADIO)". PUBLISHED:@ https://doi.org/10.1109/radio.2016.7772019

O.B Kobe, J.M Chuma "Electromagnetic analysis of variable segment width spirals on silicon substrate".

SUBMITTED TO – Microelectronics Journal – Elsevier

CHAPTER 4

4.1 CONCLUSION

A new layout optimisation method for on-chip spiral inductors is presented. The new technique is based on the variation of spiral metal width and coil spacing, and it was implemented and investigated on a square spiral. While the method is applicable to various types of spiral inductors, for analytical purposes, it is much easier to analyse it on a square spiral since it is easy to layout and is less time consuming. The new variable segment width (VSW) is an extension of the existing variable turn width (VTW) layout method. The difference between the two techniques is that the new technique varies metal width from one segment to another, with the old technique varying metal width from one turn to another. While there is a trade-off between resistance and physical size, the immediate variation of metal width brings reduced ohmic losses relating to the conducting metal.

The two models, a VTW and a VSW were built and simulated on a CST MWs Studio, where various parameters such as S, Y and Z-parameters were obtainable for evaluation of resistance, inductance and Q-factor values. Both models were simulated and optimised with a genetic algorithm (GA) in-built within the CST simulator software. The optimisation process was ran for several solver runs until the goal function values started repeating and then the optimisation process was aborted reloading the best achievable goal function value. The best parameters for each model were then recorded in Table 3.3. The optimisation results in Table 3.3 show that the VSW model requires larger area compared to the VTW model. This is due to the trace shifting from the inside as segments widths increase towards the outer turns. Also, the dielectric and substrate thickness is larger in the VSW than in the VTW, reducing electric fields created between the ground-plane and the wider metal traces, and this could increases the resonators Q-factor. Similarly, increasing the spacing between adjacent segments improves-Q, however the effect is opposite for the inductance value. With the GA, the coil spacing is as well optimised with a minimum spacing of 2.19um, and a maximum spacing of 12.55um achieved at the outer and inner turn

respectively for high-Q in the VSW model. The resulting Q-factor improvement observed was at least 35% compared to the conventional fixed width model, and 11.57% compared to the original layout optimisation technique i.e. the variable turn width and spacing. This is a very significant improvement in Q-factor, thus the new spiral exhibit better performance than the previous type.

4.2 FUTURE RECOMMENDATION

As already discussed, the existing spiral inductor models can be improved for better and stable performance over a wide frequency range.

The VSW technique can be further applied to multisided spirals such as hexagonal and octagonal for further investigations on performance trends. It is substantiated that the more the sides a spiral have the better the current distribution and performance. Therefore the expectation is that, in a multisided spiral, the VSW model can yield much better results. Despite the complexity of applying the technique to this kind of spirals, the investigation is still a necessity and should be considered for future research.

The VSW method possess high capacitive coupling, therefore it is necessary to investigate measures for dealing with the high electric fields penetrating the dielectric. A PGS technique may be considered as an additional loss compensation method to the VSW, thus a VSW model with a PGS may be considered for future work.

REFERENCES

[1] I. Rosu, "Microstrip, Stripline, and CPW Design," *YO3DAC/VA3IUL*, 1952. .

[2] R. M. Barrett and M. H. Barnes, "Microwave printed circuits," *Radio and TV News (Radio-Electronic Engineering Section) v46*, pp. 16–31, 1951.

[3] R. L. Bunch, D. I. Sanderson, and S. Raman, "Quality factor and inductance in differential IC implementations," *IEEE Microwave Magazine*, vol. 3, no. 2, pp. 2–7, 2002.

[4] J. Chen and J. Liou, "On-chip spiral inductors for RF applications: an overview," *J. Semicond. Technol. Sci.*, vol. 4, no. 3, pp. 149–167, 2004.

[5] Y. Gao, S. Z. Zardareh, X. Yang, T. X. Nan, Z. Y. Zhou, M. Onabajo, M. Liu, A. Aronow, K. Mahalingam, B. M. Howe, G. J. Brown, and N. X. Sun, "Significantly Enhanced Inductance and Quality Factor of GHz Integrated Magnetic Solenoid," *IEEE Trans. Electron Devices*, vol. 61, no. 5, pp. 1470–1476, 2014.

[6] M. Danesh, J. R. Long, R. a. Hadaway, and D. L. Harame, "A Q-factor enhancement technique for MMIC inductors," *1998 IEEE MTT-S Int. Microw. Symp. Dig. (Cat. No.98CH36192)*, vol. 1, pp. 2–5, 1998.

[7] C. Patrick Yue and S. S. Wong, "On-chip spiral inductors with patterned ground shields for Si-Based RF IC's," *IEEE J. Solid-State Circuits*, vol. 33, no. 5, pp. 743–751, 1998.

[8] K. Benaissa, J. Y. Yang, D. Crenshaw, B. Williams, S. Sridhar, J. Ai, G. Boselli, S. Zhao, S. Tang, S. Ashburn, P. Madhani, T. Blythe, N. Mahalingam, and H. S. Shichijo, "RF CMOS on high-resistivity substrates for system-on-chip applications," *IEEE Trans. Electron Devices*, vol. 50, no. 3, pp. 567–576, 2003.

[9] J. M. López-Villegas, J. Samitier, C. Cane, P. Losantos, and J. Bausells, "Improvementof the quality factor of rf integrated inductors by layout optimization," *IEEE Trans. Microw. Theory Tech.*, vol. 48, no. 1, pp. 76–83, 2000.

[10] a. R. Sorkin and E. M. Yamashev, "The lumped resonant elements in waveguides," *2001 Microw. Electron. Meas. Identification, Appl. Conf. Proceedings. MEMIA'2001 (Cat. No.01EX474)*, pp. 115–118, 2001.

[11] S. G. Negassa, "TRI-RESONATOR STRUCTURES Negassa Sori Gerba," University of Birmingham, 2012.

[12] S. Pei, Z. Wanrong, H. Lu, J. Dongyue, and X. Hongyun, "Improving the quality factor of an RF spiral inductor with non-uniform metal width and non-uniform coil spacing," *J. Semicond.*, vol. 32, no. 6, pp. 1–5, 2011.

[13] Y. C. Wu and M. F. Chang, "On-chip high-Q (>3000) transformer-type spiral inductors,"

Electron. Lett., vol. 38, no. 3, pp. 112–113, 2002.

[14] C. Hsu, C. Chen, and H. Chuang, "A 60-GHz Millimeter-Wave Bandpass Filter Using 0 . 18-μ m CMOS Technology," *IEEE Electron Device Lett.*, vol. 29, no. 3, pp. 246–248, 2008.

[15] Chaniotakis and Cory, "Frequency response: Resonance, Bandwidth, Q factor Resonance. Let's continue the exploration of the frequency response of RLC circuits by investigating the series RLC circuit shown on Figure 1.," in *Tutorial*, vol. 1, 2006, pp. 1–11.

[16] I. Rosu, "Impedance Matching," 2006.

[17] J. W. (Iowa S. U. Nilsson and S. A. (M. U. Riedel, *Electric Circuits*, 6th Editio. New Jersey: Prentice Hall, 1999.

[18] M. Gustafsson and S. Nordebo, "Bandwidth, Q Factor, and Resonance Models of Antennas," *Prog. Electromagn. Res.*, vol. 62, pp. 1–20, 2006.

[19] J. Peters, "Design of High Quality Factor Spiral Inductors in RF MCM-D," Massachusetts Institute of Technology, 2004.

[20] "chapter 6 Microwave Resonators," vol. 0, 2009.

[21] D. M. Pozar, *Microwave Engineering*, 3rd ed. John Wiley and Sons, Inc, 2005.

[22] S. Y. Liao, *Microwave Devices and Circuits*. Englewood Cliffs, N.J: Prentice Hall. Inc, 1980.

[23] T. Shim, J. P. Raskin, C. R. Neve, and M. Rais-Zadeh, "RF MEMS passives on high-resistivity silicon substrates," *IEEE Microw. Wirel. Components Lett.*, vol. 23, no. 12, pp. 632–634, 2013.

[24] K. Ben Ali, C. R. Neve, Y. Shim, M. Rais-Zadeh, and J.-P. Raskin, "Non-linear characteristics of passive elements on trap-rich high-resistivity Si substrates," *Silicon Monolith. Integr. Circuits Rf Syst. (SiRF), 2014 IEEE 14th Top. Meet.*, pp. 4–6, 2014.

[25] I. J. Bahl, "Improved quality fator spiral inductors on GaAs Substrates," *IEEE Microw. Guid. Wave Lett.*, vol. 9, no. 10, pp. 398–400, 1999.

[26] B. Guillon, D. Cros, P. Pons, K. Grenier, T. Parra, J. . Cazaux, J. . Lalaurie, J. Grafffeuil, and R. Plana, "Design and Realization of High Q Millimetre-wave Structures Through Micromachining Techniques," in *Microwave symposium Digest, 1999 IEEE MTT-S International*, 1999, no. 5.

[27] J. SUN, "Three-Dimensional Monolithic MEMS Coil," University of Cincinnati, 2003.

[28] J. Bertinet, E. Leleux, J. Cazenave, and T. Microelectronics, "Filtering Capacitor Embedded in LTCC Substrate for RF and Microwave Applications," *Microw. J.*, vol. 1, no. 11, pp. 1–11, 2007.

[29] J. Mazierska, M. V. Jacob, A. Harring, J. Krupka, P. Barnwell, and T. Sims, "Measurements of loss tangent and relative permittivity of LTCC ceramics at varying temperatures and

frequencies," *J. Eur. Ceram. Soc.*, vol. 23, no. 14, pp. 2611–2615, 2003.

[30] L. Devlin, G. Pearson, J. Pittock, and B. Hunt, "RF and Microwave Components in LTCC," vol. 44, no. 0, 2001.

[31] L. J. Golonka, "Technology and applications of Low Temperature Cofired Ceramic (LTCC) based sensors and microsystems," *Bull. Polish Acad. Sci. - Tech. Sci.*, vol. 54, no. 2, pp. 221–231, 2006.

[32] L. Golonka, P. Bembnowicz, D. Jurków, K. Malecha, H. Roguszczak, and R. Tadaszak, "Low temperature co-fired ceramics (LTCC) microsystems," *Opt. Appl.*, vol. 41, no. 2, pp. 383–388, 2011.

[33] J. Ganne, M. Paté, and R. Lebourgeois, "Filtering Capacitor with Bi-Zn-Oxide Dielectric Embedded in a LTCC Substrate," no. November, pp. 1–6, 2007.

[34] N. M. Nguyen and R. G. Meyer, "Si IC-compatible inductors and LC passive filters," *IEEE J. Solid-State Circuits*, vol. 27, no. 8, pp. 1028–1031, 1990.

[35] A. M. Niknejad, S. Member, and R. G. Meyer, "Analysis , Design , and Optimization of Spiral Inductors and Transformers for Si RF IC ' s," vol. 33, no. 10, pp. 1470–1481, 1998.

[36] C. Pacurar, V. Topa, A. Racasan, C. Munteanu, and C. Hebedean, "Spiral Inductors Analysis and Modelling," pp. 210–215, 2014.

[37] G. Yacine, R. Mohamed, and H. Azzedine, "Design and Modeling of a Square Planar Inductor for a Push Pull Converter," p. 17.

[38] C. Pacurar, V. Topa, A. Racasan, C. Munteanu, C. Hebedean, and D. Rafiroiu, "High Frequency Modeling of Square Spiral Inductor," in *International Conference and Exposition on Electrical and Power Engineering (EPE 2014), 16-18 October, Lasi, Romania*, 2014, no. 10, pp. 622–626.

[39] K. Okada and K. Masu, "Modeling of Spiral Inductors," pp. 291–313.

[40] J. Shi, W. Y. Yin, H. Liao, and J. F. Mao, "The enhancement of Q factor for patterned ground shield inductors at high temperatures," *IEEE Trans. Magn.*, vol. 42, no. 7, pp. 1873–1875, 2006.

[41] J. Craninckx and M. S. . Steyaert, "A 1.8 GHz low phase-noise CMOS VCO using optimized hollow spiral inductors," *IEEE J. Solid-State Circuits*, vol. 32, no. 5, pp. 736–744, 1997.

[42] V. Narayana, R. Vanukuru, and A. Chakravorty, "High- Q Characteristics of Variable Width Inductors With Reverse Excitation," *IEEE Trans. Electron Devices*, vol. 61, no. 9, pp. 3350–3354, 2014.

[43] R. R. Manikandan, V. Narayana, R. Vanukuru, A. Chakravorty, and B. Amrutur, "A Parameterized Cell Design for High-Q , Variable Width and Spacing Spiral Inductors," in

IEEE International Microwave and RF Conference, 2014, pp. 312–315.

[44] F. Passos, M. H. Fino, and R. Moreno, Elisenda, "Analythical Characterization of Variable Width Integrated Spiral Inductors," in *International Conference "Mixed Design of Integrated Circuits and systems,"* 2013, pp. 586–591.

[45] K. Murata, T. Hosaka, and Y. Sugimoto, "Effect of ground shield on silicon on-chip spiral inductor," in *Microwave Conference,2000 Asia-Pacific*, 2000.

[46] T. Zheng, M. Han, G. Xu, and L. Luo, "A Novel WL-Integrated Low-Insertion-Loss Filter with Suspended High- Q Spiral Inductor and Patterned Ground Shields," *Prog. Electromagn. Res. C*, vol. 59, no. August, pp. 41–49, 2015.

[47] R. Pokharel and X. Liu, "A high selectivity, low insertion loss 60GHz-band on-chip 4-pole band pass filter for millimeter wave CMOS SoC," *2011 Eur. Microw. Integr. Circuits Conf.*, no. October, pp. 660–663, 2011.

[48] M. T. Reiha, T.-Y. Choi, J.-H. Jeon, S. Mohammadi, and L. P. B. Katehi, "High-Q Differential Inductors for RFIC Design," *Microw. Conf. 2003. 33rd Eur.*, pp. 127–130, 2003.

[49] M. Danesh and J. R. Long, "Differentially Driven Symmetric Microstrip Inductors," *IEEE Trans. Microw. Theory Tech.*, vol. 50, no. 1, pp. 332–341, 2002.

[50] W. B. Kuhn, S. Member, X. He, S. Member, and M. Mojarradi, "Modeling Spiral Inductors in SOS Processes," *IEEE Trans. Electron Devices*, vol. 51, no. 5, pp. 677–683, 2004.

[51] K. D. Pham, K. Okada, and K. Masu, "Quality Factor Enhancement of On-Chip Inductor by Using Negative Impedance Circuit," in *Silicon Monolithic Integrated Circuits in Rf Systems, 2006. Digest of papers, 2006 Topical Meeting on*, 2006, pp. 115–118.

[52] T. Soorapanth and S. Wong, "A 0-dB IL 2140 +/- 30 MHz bandpass filter utilizing Q-enhanced spiral inductors in standard CMOS," *IEEE J. Solid-State Circuits*, vol. 37, no. 5, pp. 579–586, 2002.

[53] R. R. Manikandan, R. Vanukuru, V. Narayana, A. Chakravorty, and B. Amrutur, "Design and modeling of high-Q variable width and spacing, planar and 3-D stacked spiral inductors," *18th Int. Symp. VLSI Des. Test*, pp. 1–6, 2014.

[54] U. Yodprasit and J. Ngarmnil, "Q-enhancing technique for rf CMOS active inductor," *2000 IEEE Int. Symp. Circuits Syst. Geneva, Switz.*, no. 5, pp. 589–592, 2000.

[55] C. Andriesei and L. Goras, "On frequency and quality factor independent tuning possibilities for rf band-pass filters with simulated inductors," *Rom. J. Inf. Sci. Technol.*, vol. 11, no. 4, pp. 367–382, 2008.

[56] S. Bantas and Y. Koutsoyannopoulos, "CMOS Active-LC Bandpass Filters With Coupled-Inductor Q-Enhancement and Center Frequency Tuning," *IEEE Trans. Circuits Syst. II*

Analog Digit. Signal Process., vol. 51, no. 2, pp. 69–76, 2004.

[57] D. Beifort, N. Beilleau, H. Aboushady, M. M. Louërat, and S. Catunda, "A Q-Enhanced LC bandpass filter using CAIRO+," *2009 16th IEEE Int. Conf. Electron. Circuits Syst. ICECS 2009*, no. 3, pp. 860–863, 2009.

[58] S. Wang and R. X. Wang, "A Tunable Bandpass Filter Using Q-enhanced and semi-passive inductor at S-Band in 0.18um CMOS," *Prog. Electromagn. Res. B, Vol. 28, 55–73, 2011*, vol. 28, no. January, pp. 55–73, 2011.

[59] B. Georgescu, H. Pekau, J. Haslett, and J. McRory, "Tunable coupled inductor Q-enhancement for parallel resonant LC tanks," *IEEE Trans. Circuits Syst. II Analog Digit. Signal Process.*, vol. 50, no. 10, pp. 705–713, 2003.

[60] A. Naderi, M. Sawan, and Y. Savaria, "A 1-mW 2-GHz Q-enhanced LC bandpass filter for low-power RF applications," *3rd Int. IEEE Northeast Work. Circuits Syst. Conf. NEWCAS 2005*, vol. 2005, pp. 365–368, 2005.

[61] J. Keech, G. Piech, S. Pollard, S. Chaparala, A. Shorey, and B. K. Wang, "Glass Interposer Substrates : Fabrication , Characterization and Modeling," in *Electronics Packaging Technology Conference*, 2013, no. 88, pp. 706–709.

[62] W. SHANG, C. PANG, Z. QIN, D. YU, and D. SHANGGUAN, "Modeling, Simultion and Analysis of Coplanar Waveguide on Glass Substrate for 2.5D Integration," in *2014 15th International Conference on Electronics Packaging Technology*, 2014, pp. 564–567.

[63] X. Gu, R. Rimolo-donadio, R. Budd, C. W. Baks, C. Jahnes, D. M. Kuchta, C. L. Schow, and F. Libsch, "High-Speed Signaling Performance of Multilevel Wiring on Glass Substrates for 2 . 5-D Integrated Circuit and Optoelectronic Integration," in *Electronic Components & Technology Conference*, 2013, pp. 846–851.

[64] S. Cho, Y. Joshi, V. Sundaram, Y. Sato, and R. Tummala, "Comparison of Thermal Performance between Glass and Silicon Interposers," *Eletronic Components Technol. Conf.*, pp. 1480–1487, 2013.

[65] V. Sukumaran, T. Bandyopadhyay, Q. Chen, N. Kumbhat, F. Liu, R. Pucha, and Y. Sato, "Design , Fabrication and Characterization of Low-Cost Glass Interposers with Fine-Pitch Through-Package-Vias," in *2011 Electronic Components and Technology Conference*, 2011, pp. 583–588.

[66] V. Sukumaran, Q. Chen, F. Liu, N. Kumbhat, T. Bandyopadhyay, H. Chan, S. Min, C. Nopper, V. Sundaram, and R. Tummala, "Through-Package-Via Formation and Metallization of Glass Interposers," in *Electronic Components & Technology Conference*, 2010, pp. 557–563.

[67] V. Sridharan, S. Min, V. Sundaram, V. Sukumaran, S. Hwang, H. Chan, F. Liu, C. Nopper, and R. Tummala, "Design and Fabrication of Bandpass Filters in Glass Interposer with Through-Package-Vias (TPV)," in *2010 Proceedings 60th Electronic Components and Technology Conference (ECTC)*, 2010, pp. 530–535.

[68] G. R. Trott and A. Shorey, "Glass wafer mechanical properties: A comparison to silicon," *2011 6th Int. Microsystems, Packag. Assem. Circuits Technol. Conf.*, no. Lcd, pp. 359–362, 2011.

[69] I. 2016 ANSYS, "ANSYS HFSS High Frequency Electromagnetic Field Simulation," 2016. [Online]. Available: http://www.ansys.com/Products/Electronics/ANSYS-HFSS. [Accessed: 26-Oct-2016].

[70] G. A. E. Vandenbosch and A. Vasylchenko, "A Practical Guide to 3D Electromagnetic Software Tools," *INTECH Open Access*, 2011. [Online]. Available: www.intechopen.com/books/microstrip-antennas.

[71] A. B. Islam, S. K. Islam, and F. S. Tulip, "Design and Optimization of Printed Circuit Board Inductors for Wireless Power Transfer System," vol. 2013, no. April, pp. 237–244, 2013.

[72] I. 2016 Sonnet Software, "3D Planar High-Frequency Electromagnetic Software," 2016. [Online]. Available: http://www.sonnetsoftware.com/products/sonnet-suites/. [Accessed: 26-Oct-2016].

[73] 2016 CST Computer Simulation Technology AG, "CST STUDIO SUITE," 2016. [Online]. Available: https://www.cst.com/products/csts2. [Accessed: 26-Oct-2016].

[74] K. A. Othman, Z. I. Khan, S. A. Kadri, and N. Hamzah, "Q-Factor Evaluation of Spiral Inductor for 5.8GHz WiMAX Application," in *Proceedings of the World Congress on Engineering 2011*, 2011, vol. II, pp. 6–9.

[75] 2016 CST Computer Simulation Technology AG, "CST MICROWAVE STUDIO," 2016. [Online]. Available: https://www.cst.com/products/cstmws. [Accessed: 26-Oct-2016].

[76] G. Crevecoeur, P. Sergeant, L. Dupré, R. Van De Walle, and A. Metamodels, "A Two-Level Genetic Algorithm for Electromagnetic Optimization," *IEEE Trans. Magn.*, vol. 46, no. 7, pp. 2585–2595, 2010.

[77] R. L. Haupt, "An Introduction to Genetic Algorithms for Electromagnetics," *IEEE Antennas Propag. Mag.*, vol. 37, no. 2, pp. 7–15, 1995.

[78] F. J. Villegas, T. Cwik, Y. Rahmat-samii, and M. Manteghi, "A Parallel Electromagnetic Genetic-Algorithm Optimization (EGO) Application for Patch Antenna Design," *IEEE Trans. Antennas Propag.*, vol. 52, no. 9, pp. 2424–2435, 2004.

[79] A. M. Niknejad, "ANALYSIS , DESIGN , AND OPTIMIZATION OF SPIRAL

INDUCTORS AND TRANSFORMERS FOR SI RF ICS," College of Engineering, University of California, Berkeley.

[80] C. P. Yue, C. Ryu, J. Lau, T. H. Lee, and S. S. Wong, "A physical model for planar spiral inductors on silicon," *Int. Electron Devices Meet. Tech. Dig.*, pp. 155–158, 1996.

[81] J.-C. Guo, "Analytical modeling of proximity and skin effects for millimeter-wave inductors simulation and design in nano Si CMOS," *2014 IEEE MTT-S Int. Microw. Symp.*, vol. 0, no. 2, pp. 1–4, 2014.

[82] N. A. Talwalkar, C. P. Yue, and S. S. Wong, "Analysis and Synthesis of On-Chip Spiral Inductors," *IEEE Trans. Electron Devices*, vol. 52, no. 2, pp. 176–182, 2005.

[83] M. Kosek, M. Truhlar, and A. Richter, "Skin-effect in Conductor of Rectangular Cross-section — Approximate Solution," *Prz. ELEKTROTECHNICZNY (Electrical Rev.*, no. 7, pp. 23–25, 2012.

[84] A. M. Niknejad and R. G. Meyer, "Analysis of Eddy-Current Losses Over Conductive Substrates with Applications to Monolithic Inductors and Transformers," *IEEE Trans. Microw. Theory Tech.*, vol. 49, no. 1, pp. 166–176, 2001.

[85] P. Almeida, P. Pereira, and H. Fino, "Using Variable Width RF Integrated Inductors for Quality Factor Optimization," in *4th Doctoral Conference on Computing, Electrical and Industrial Systems (DoCEIS), Apr 2013, Costa de Caparica, Portugal*, 2013, pp. 613–621.

[86] V. Narayana, R. Vanukuru, and R. Groves, "Layout Optimized Non-Uniform Series-Parallel Inductors for High Inductance Density and Quality Factor," pp. 748–751, 2015.

APPENDIX A

A.1. PUBLICATIONS

1. O.B. Kobe et al., "A review on quality factor enhanced on-chip microwave planar resonators, Eng. Sci. Tech., Int. J. (2016), Elsevier".
   http://dx.doi.org/10.1016/j.jestch.2016.09.024

2. O.B. Kobe et al. "Modelling high-Q square spiral with variable segment width and spacing, 2016 IEEE Radio and Antenna days of the Indian Ocean (RADIO)".
   https://doi.org/10.1109/radio.2016.7772019

3. O.B Kobe, J.M Chuma "Electromagnetic analysis of variable segment width and spacing spirals on silicon substrate".
   Submitted to: Microelectronics Journal – Elsevier

A.2. OPTIMISATION RUN

i) Variable Turn Width Spiral Inductor

The automatically added space for open boundaries has been limited to ten times the model's bounding box diagonal because the structure is very small in terms of the smallest wavelength.

Meshing successful

The mesh adaptation has been deactivated. It is strongly recommended to enable the mesh adaptation for the tetrahedral mesh unless the problem is very large.

Sample 1 (4 GHz)

Automatically activated electric shielding for ports 1, 2.

Performing parallel excitation with 2 threads. More...

Stimulation at port 1, mode 1

Stimulation at port 2, mode 1

Sample 2 (1 GHz)

Stimulation at port 1, mode 1

Stimulation at port 2, mode 1

Sample 3 (2.2 GHz)

Stimulation at port 1, mode 1

Stimulation at port 2, mode 1

Sample 4 (1.8 GHz)

Stimulation at port 1, mode 1

Stimulation at port 2, mode 1

Sample 5 (2 GHz)

Stimulation at port 1, mode 1

Stimulation at port 2, mode 1

No automatic samples have been calculated up to now. Therefore, the frequency sweep is continued with additional automatically chosen samples.

Sample 6 (3.439 GHz)

Stimulation at port 1, mode 1

Stimulation at port 2, mode 1

Sample 7 (1.213 GHz)

Stimulation at port 1, mode 1

Stimulation at port 2, mode 1

Sample 8 (2.887 GHz)

Stimulation at port 1, mode 1

Stimulation at port 2, mode 1

The S-parameter convergence criterion has been satisfied after calculating 8 frequency samples.

Calculating remaining monitors.

The Z and Y matrices have been successfully calculated.

The VSWR results have been successfully calculated.

Parametric 1D storage is switched off.

The automatically added space for open boundaries has been limited to ten times the model's bounding box diagonal because the structure is very small in terms of the smallest wavelength.

Optimization aborted with improved goal value. Best parameter set is stored.

ii) Variable Segment Width Spiral Inductor

The automatically added space for open boundaries has been limited to ten times the model's bounding box diagonal because the structure is very small in terms of the smallest wavelength.

Generating a finer mesh for listed regions or removing small features may help. More...

Meshing successful

The mesh adaptation has been deactivated. It is strongly recommended to enable the mesh adaptation for the tetrahedral mesh unless the problem is very large.

Sample 1 (4 GHz)

Automatically activated electric shielding for ports 1, 2.

Performing parallel excitation with 2 threads. More...

Stimulation at port 1, mode 1

Stimulation at port 2, mode 1

The direct solver will be used.

Sample 2 (1 GHz)

Stimulation at port 1, mode 1

Stimulation at port 2, mode 1

Sample 3 (2.2 GHz)

Stimulation at port 1, mode 1

Stimulation at port 2, mode 1

Sample 4 (1.8 GHz)

Stimulation at port 1, mode 1

Stimulation at port 2, mode 1

Sample 5 (2 GHz)

Stimulation at port 1, mode 1

Stimulation at port 2, mode 1

No automatic samples have been calculated up to now. Therefore, the frequency sweep is continued with additional automatically chosen samples.

Sample 6 (3.598 GHz)

Stimulation at port 1, mode 1

Stimulation at port 2, mode 1

An additional check has indicated that the frequency sweep needs to be continued.

Sample 7 (1.285 GHz)

Stimulation at port 1, mode 1

Stimulation at port 2, mode 1

Sample 8 (2.17 GHz)

Stimulation at port 1, mode 1

Stimulation at port 2, mode 1

The iterative solver will be used.

The S-parameter convergence criterion has been satisfied after calculating 8 frequency samples.

Calculating remaining monitors.

The Z and Y matrices have been successfully calculated.

The VSWR results have been successfully calculated.